International Journal of Earth Sciences (2023) 112:1635–1660
https://doi.org/10.1007/s00531-023-02321-6

ORIGINAL PAPER

Late Alpine multistage exhumation of the northwestern Rhodope Metamorphic Complex (northern Rila Mountains, Bulgaria)

Alexandre Kounov[1] · Ianko Gerdjikov[2] · Milorad D. Antić[3] · Neven Georgiev[2] · Richard A. Spikings[4]

Received: 5 July 2022 / Accepted: 17 May 2023 / Published online: 2 June 2023

Abstract

The Rhodope crystalline massif is an Alpine metamorphic complex exposed across several mountain ranges in southern Bulgaria and northern Greece which has experienced a complex history including continental collision, partial subduction and syn-metamorphic nappe stacking followed by syn- to post-contractional extension. We present new $^{40}Ar/^{39}Ar$ and fission-track data from samples taken from both sides of the North Rhodopean Detachment that were combined with detailed structural studies to investigate the tectonothermal evolution of the northern Rila Mountains. A migmatite from the hanging wall of the North Rhodopean Detachment yields a $^{40}Ar/^{39}Ar$ muscovite age of 100.79 ± 0.55 Ma, a zircon fission-track age of 38.6 ± 1.9 Ma, and an apatite fission-track age of 21.4 ± 1.5 Ma. A biotite schist from the footwall of the detachment yields $^{40}Ar/^{39}Ar$ biotite age of 34.90 ± 0.15 Ma, and zircon and apatite fission-track ages of 35.6 ± 5.6 and 13.3 ± 1.1 Ma, respectively. Our new data give evidence of a multistage exhumation of the study area. Late Early Cretaceous (~ 101 ± 0.6 Ma) cooling of the Variscan high-grade metamorphic basement through 440–400 °C was caused by either erosion of the emplacing thrust sheet, or post-contractional denudation. Fast exhumation along the North Rhodopean Extensional System drove a pulse of increased tectonic denudation and cooling during the Eocene (39–35 Ma). Exhumation of the rocks in the northern part of the Rila Mountains below 110 ± 10 °C during the middle–late Miocene was associated with displacement along a system of normal faults.

Keywords Rhodope Metamorphic Complex · Rila Mountains · North Rhodopean Extensional System · North Rhodopean Detachment · $^{40}Ar/^{39}Ar$ and FT analysis · Thrusting · Extension

Introduction

The Rhodope Metamorphic Complex (RMC) is exposed in several mountain ranges in southern Bulgaria and northern Greece, including the Rhodope, Rila, Pirin, Vrontous and Pangaion mountains (Fig. 1). In general, the geology of the Rhodope Mountains has attracted far more attention than some other parts of the complex, e.g. the Pirin and Rila Mountains. One probable reason for this is simply accessibility. The Pirin and Rila Mountains, culminating at 2925 m, are the highest and least accessible parts of the Rhodope Metamorphic Complex (Fig. 2). Extensive research in the Rhodope Mountains during the previous 30 years reveals a complex Alpine age (Late Jurassic to Quaternary) tectonic evolution that includes continental collision, partial subduction and syn- to post-contractional crustal extension (e.g. Burg et al. 1995, 1996; Dinter and Royden 1993; Dinter 1998; Ricou et al. 1998; Burg 2012; Froitzheim et al. 2014). In comparison, geochronological and structural studies of the rocks exposed in the Rila and Pirin mountains are relatively scarce and only partly elucidates the tectonic evolution of the northwestern Rhodope Metamorphic Complex (Dimov and Damianova 1996; Shipkova and Ivanov 2000; Tueckmantel et al. 2008; Gunnell et al. 2017; Gorinova et al. 2019). The results of this limited research indicate at least two major Alpine contractional events (Gorinova et al. 2019), followed by a period of extension, which drove exhumation

✉ Alexandre Kounov
a.kounov@unibas.ch

[1] Department of Environmental Sciences, Basel University, 4056 Basel, Switzerland

[2] Faculty of Geology and Geography, St. Kliment Ohridski University, 1000 Sofia, Bulgaria

[3] Zlatna Reka Resources, 11167 Belgrade, Serbia

[4] Section des Sciences de la Terre et de l'Environnement, Université de Genève, 1205 Geneva, Switzerland

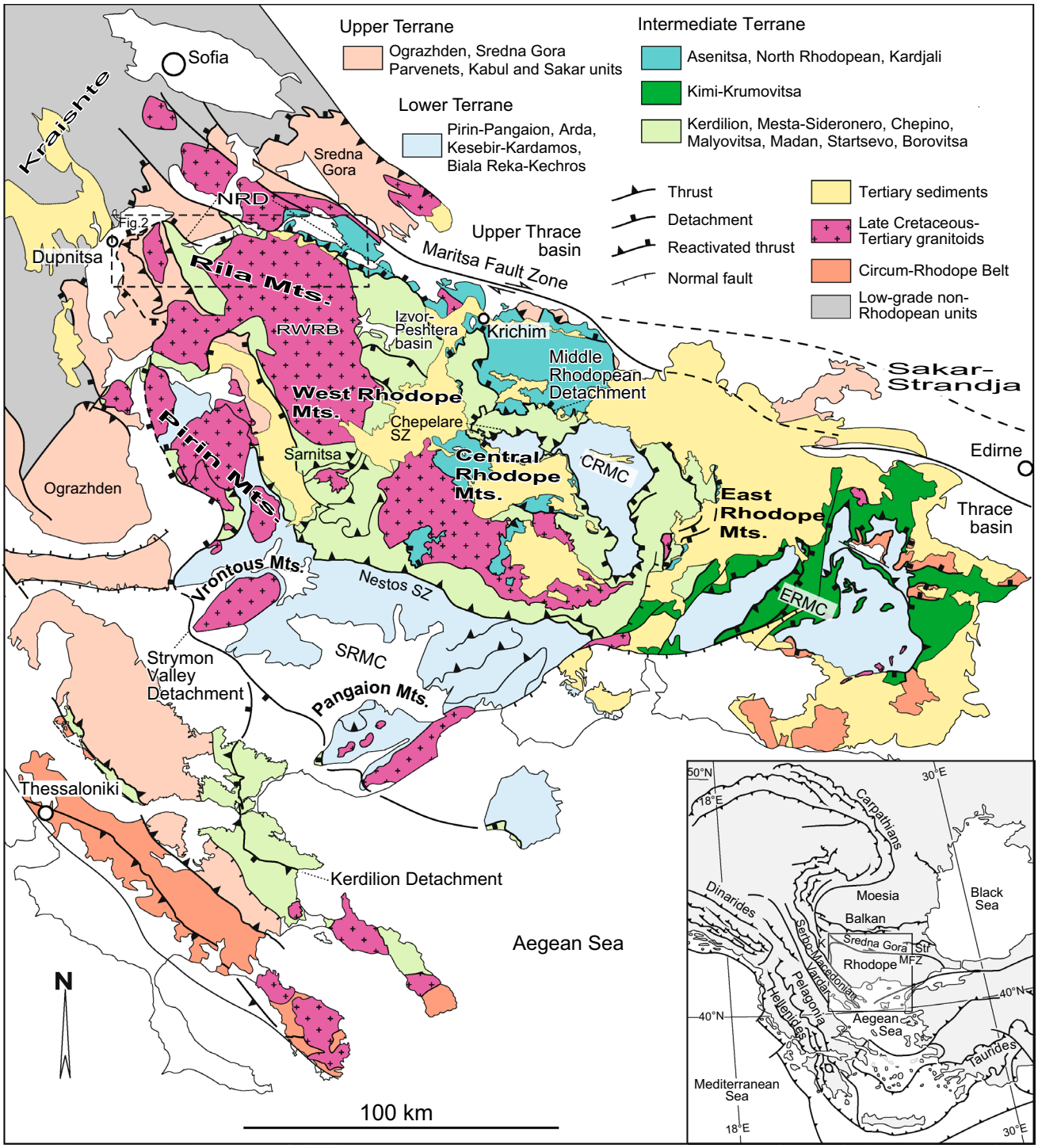

Fig. 1 Sketch map of the Rhodope Metamorphic Complex (modified after Burg 2012). The box outlines Fig. 2. CRMC Central Rhodope Metamorphic Complex. SRMC South Rhodope Metamorphic Complex. ERMC Eastern Rhodope Metamorphic Complex. *K* Kraishte area, *Str* Strandja zone, *MFZ* Maritsa Fault Zone, *RWRB* Rila–West Rhodope Batholith, *NRD* North Rhodopean Detachment

along a detachment fault (Shipkova and Ivanov 2000; Gerdjikov et al. 2006; Tueckmantel et al. 2008; Gorinova et al. 2019). In the Rila Mountains, rocks of the Lower Terrane are not exhumed, unlike the central, east and southern parts of the Rhodope Metamorphic Complex (Fig. 1, Gorinova et al. 2019). Furthermore, the rocks exposed in the Rila Mountains exhibit no evidence of syn-extensional migmatisation, characteristic for other parts of the metamorphic complex

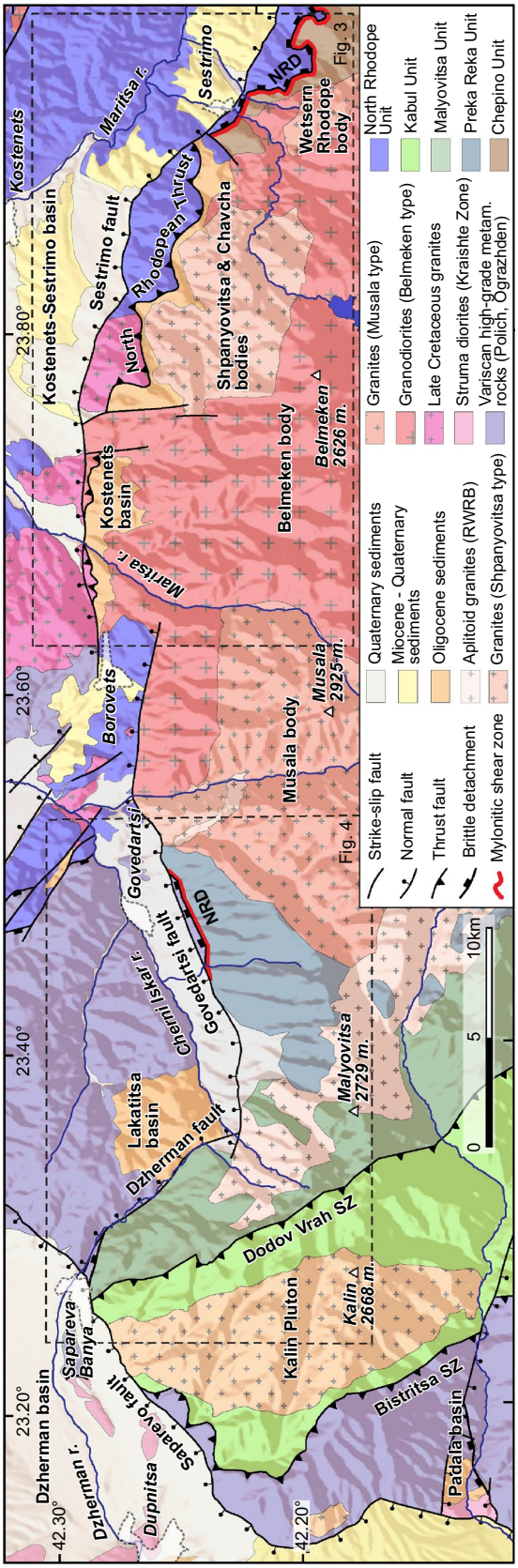

Fig. 2 Geological map of the northern Rila Mountains (modified after 1:50,000 geological maps of Bulgaria). The boxes outline Figs. 3, 4. NRD: North Rhodopean Detachment

(Gorinova et al. 2019), suggesting the area probably escaped these high-temperature/high-pressure Alpine events.

This paper presents new structural and thermochronological (fission-track and $^{40}Ar/^{39}Ar$) data that constrain the late Alpine tectonic evolution of the northwestern Rhodope Metamorphic Complex exposed in the northern parts of the Rila Mountains. Integration of the new data with other previously published data reveal a multistage extensional evolution of the region comprising at least two major phases of exhumation. An initial early phase of very fast exhumation along a ductile to brittle crustal-scale detachment, the North Rhodopean Detachment (Fig. 1), during the late Eocene (39–35 Ma). A second, later phase of exhumation, beginning in the middle to late Miocene and continuing even in the Quaternary, is accommodated by displacement along brittle, high-angle normal faults that are responsible for the final uplift and creation of the present-day Rila and Pirin high-mountain ranges. These two episodes of major extension are separated by an intervening subordinate phase of strike-slip to thrust tectonics, which is probably responsible for some reheating that is observed in all the new rock samples analysed herein as well as those analysed in previous studies.

The multidisciplinary, structural and thermochronological, analytical methodology this paper employs provide additional degrees of constraint for interpretation of the Cenozoic tectonic evolution of the area, which facilitates determination of the age, distinct structural style of deformation and likely plate tectonic setting of each discrete episode of exhumation and uplift or burial. Analyses of the first phase of Late Eocene age exhumation of middle to lower crustal rocks associated with the formation of crustal-scale, low-angle, ductile to brittle detachment faults accommodating regional extension, suggested deformation in a subduction-related plate tectonic setting. Whilst the second phase of exhumation and uplift, creating the present-day high-mountain topographic relief, associated with the formation of brittle, high-angle normal faults and continental basins is most likely associated with a change in tectonic setting from orogenic subduction to a post-orogenic crustal thinning, inferring a reorganisation of the plate boundaries at this time.

Regional geology

Rhodope metamorphic complex

The Rhodope high-grade metamorphic complex, exposed in southern Bulgaria and northern Greece, represents an Alpine syn-metamorphic nappe stack that experienced massive crustal extension and core complex formation during the Cenozoic (Fig. 1). Although several different tectono-metamorphic subdivisions were suggested (e.g. Burg et al. 1996; Turpaud and Reischmann 2010; Janák et al. 2011; Burg 2012; Kydonakis et al. 2015; Schmid et al. 2020), there is general consensus that the metamorphic complex is composed of three main terranes that were initially juxtaposed during a Cretaceous (e.g. Ricou et al. 1998; Burg 2012; Bonev et al. 2015) or Cenozoic collision (e.g. Dinter 1998; Nagel et al. 2011; Froitzheim et al. 2014; Gorinova et al. 2019; Fig. 1). A Lower and Upper terrane represent continental fragments separated by an Intermediate terrane, which has a Jurassic ophiolitic and magmatic arc protolith (e.g. Burg 2012). All of these Rhodopean terranes contain ultra- to high-grade/high-pressure metamorphic rocks, some of which are reported to be of Alpine ages (Liati 2005; Liati et al. 2002; Bosse et al. 2010; Georgieva et al. 2011; Kirchenbaur et al. 2012; Kydonakis et al. 2015; Petrik et al. 2016; Collings et al. 2016). Two differing models were proposed concerning the time of the major orogeny leading to the tectonic juxtaposition of the Rhodopean terranes (e.g. Ricou et al. 1998; Dinter 1998; Nagel et al. 2011; Burg 2012; Froitzheim et al. 2014; Bonev et al. 2015; Gorinova et al. 2019). The first one suggests a single, Late Jurassic–Early Cretaceous, major orogenic episode of northward subduction (e.g. Burg 2012) whereas, the second envisages a two-step scenario, comprising an initial north-vergent Late Jurassic arc-continent collision, followed by Eocene–Oligocene south-vergent continent–continent collision (e.g. Froitzheim et al. 2014; Petrik et al. 2016). The model presented by Gautier et al. (2017) also distinguishes two orogenic cycles in the evolution of the Rhodope metamorphic complex, one of Late Jurassic–Early Cretaceous age and the other of Late Cretaceous–Cenozoic time age, which are separated by ~45 Myr (117–70 Ma) period of relative tectonic quiescence.

Eocene–Oligocene syn- to post-contractional extension followed by Miocene post- contractional extension generated core complexes that are bound by gently dipping detachment faults (e.g. Dinter and Royden 1993; Krohe and Mposkos 2002; Bonev et al. 2006; Brun and Sokoutis 2007; Georgiev et al. 2010, 2016; Kounov et al. 2015, 2020) with cores mainly comprising rocks of the Lower Terrane (Fig. 1). Different names were attributed to these extensional core complexes, whereas we group them here in three major metamorphic complexes—Central, Southern and Eastern (Fig. 1, Kounov et al. 2020).

The extension was also associated with formation of grabens that are filled with Eocene to Quaternary marine to continental deposits (e.g. Cernjavska 1977; Ivanov et al. 2000), accompanied by volcanic and intrusive magmatism (e.g. Harkovska et al. 1998; Marchev et al. 2005). Ductile southward syn-extensional thrusting along the Chepelare and Nestos shear zones (Fig. 1) as young as 36 Ma was also reported, suggesting that the deeper crustal levels of the Rhodope Metamorphic Complex were still accommodating

shortening until at least this time (Bosse et al. 2009; Jahn-Awe et al. 2012; Nagel et al. 2011; Gautier et al. 2017).

Rila Mountains

For the Rila Mountains, which occupy the northwestern corner of the Rhodope Metamorphic Complex (Figs. 1 and 2), several slightly diverging tectonometamorphic subdivisions were suggested (Dimov and Damianova 1996; Sarov et al. 2011a; Gorinova et al. 2019). However, there is common agreement that all the units have experienced a major tectonometamorphic event during Alpine time, except the uppermost Variscan high-grade metamorphic rocks (Fig. 2, Sarov et al. 2011a). The main units exposed in the northwestern part of Rila Mountains are Kabul, Malyovitsa and Preka Reka units, whilst the multiphase Rila–West Rhodope Batholith occupies the central and eastern parts (71–39 Ma, von Quadt and Peytcheva 2005; Peytcheva et al. 2007; Figs. 1 and 2). The Chepino Unit, which is previously considered to be part of the Intermediate (Sarov et al. 2008a, Fig. 2) or the Lower Rhodopean terranes (Burg 2012), crops out in the easternmost margin of the Rila Mountains where it is overlain by the North Rhodopean Unit of the Upper Rhodopean Terrane (Burg 2012, Fig. 2) above the North Rhodopean Detachment (Gerdjikov et al. 2006). Below, the units exposed in the study area and the composition of the North Rhodopean Extensional System (Gerdjikov et al. 2006) are described in more detail.

Chepino Unit

The exact structural position of the unit in the Rhodopean crustal stack is unclear. However, Maastrichtian–early Paleocene (63–59 Ma) monazite ages from a leucosome (Cherneva et al. 2006), giving evidence for Alpine migmatisation, suggests a lowermost tectonic position in the Rila Mountains. The unit is composed of migmatized biotite and amphibole–biotite gneisses, thin marble packages and lenses of amphibolites, all of which are affected by upper amphibolite-facies metamorphism at temperatures of 600–650 °C associated with partial melting (Sarov et al. 2008a).

The metamorphic foliation in the study area dips shallowly to the northeast and east–northeast, with stretching lineations that plunge towards the north–northeast (Sarov et al. 2008a). Sense-of-shear criteria record both top-to-the-south and southeast, as well as top-to-the-north and northwest syn-metamorphic tectonic transport. Interpretation of these opposite directed senses-of-shear infer a complex tectonic evolution, which includes initial south-vergent thrusting followed by northward directed extension and the formation of the North Rhodopean Extensional System during the late Eocene (Gerdjikov and Gautier 2006; Gerdjikov et al. 2006).

Preka Reka and Malyovitsa Units

The relationship between the Malyovitsa and Preka Reka units with the Chepino Unit is unclear, because they are separated by the Rila–West Rhodope Batholith (RWRB, Fig. 2). The Preka Reka Unit (Gorinova et al. 2019) mainly consists of orthogneisses and the overlying Malyovitsa Unit comprise paragneisses, orthogneisses, amphibolites, marbles, schists and metaultrabasic rocks (e.g. Dimov and Damianova 1996) (Fig. 2). Dimov and Damianova (1996) reported top-to-the-southeast displacement along the ductile Malyovitsa Shear Zone that separates both units. Gorinova et al. (2019) consider both units are part of the same litho-tectonic body (the "Malyovitsa Unit"), even though they are separated by a ductile shear zone, because granites of the Preka Reka Unit intrude the Malyovitsa Unit para-series. Gorinova et al. (2019) also interpret the Malyovitsa Unit is regionally very similar to Sarnitsa Unit, which outcrops roughly 100 km south–southeast, to the south of the RWRB (Sarov et al. 2010, Fig. 1).

The protolith for the orthogneisses of the Preka Reka Unit is reportedly Late Jurassic to Early Cretaceous age (156–135 Ma U–Pb zircon ages, Popov and Ivanov 2012; Gorinova et al. 2019). The unit is subsequently intruded by both Late Cretaceous (71 Ma) granodiorites and Eocene (39 Ma) granites of the RWRB (von Quadt and Peytcheva 2005; Peytcheva et al. 2007; Fig. 2). The rocks of the Malyovitsa and Preka Reka units underwent moderate amphibolite-facies metamorphism with no evidence of a high-pressure event (Gorinova et al. 2019). Gorinova et al. (2019) described an older metamorphic fabric, related to an early Late Cretaceous tectonometamorphic event, which was isoclinally folded during the development of the axial planar foliation that is the main penetrative fabric in both units. A U–Pb concordia age of ca. 82 Ma obtained from recrystallised rims of zircon crystals from the Jurassic orthogneiss body (Gorinova et al. 2019) is interpreted to date the earlier amphibolite-facies metamorphic event. Based on syn-kinematic granitic dykes and veins, the formation of the second main fabric in the Malyovitsa Unit is fixed between 51 and 48 Ma, contemporaneous to the movement along the Dodov Vrah Shear Zone (Fig. 2, Gorinova et al. 2019). This foliation dips moderately to the southwest or west and bears a subhorizontal northwest–southeast-trending stretching lineation that is parallel to the fold axes of the isoclinal folds. Kinematic indicators reveal a syn-metamorphic, top-to-the-southeast sense-of-shear (Dimov and Damianova 1996; Shipkova 1999; Gorinova et al. 2019).

Kabul Unit

The Kabul Unit is composed of amphibolite-facies paragneisses and orthogneisses that show evidence for migmatisation, and also hosting large bodies of amphibolites and relics of eclogites (Dimitrova 1960; Kolcheva and

Cherneva 1999; Gorinova et al. 2019). These rocks yield Ediacaran–Cambrian protolith ages and also include relics of Permian–Triassic high-pressure rocks. All the rocks are overprinted by high-temperature metamorphism (Miladinova et al. 2013; Gorinova 2020) with calculated PT conditions of ≤ 650 °C/0.7–0.8 GPa to 460–500 °C/0.1–0.3 GPa for the metapelites (Kolcheva and Cherneva 1999).

The main penetrative foliation in the Kabul Unit dips to the southwest or northeast. Fold axes plunge at low angles to the northwest or southeast. The foliation bears mostly a northwest–southeast-trending stretching lineation. Kinematic indicators in the non-folded domains show a top-to-the-north–northwest sense-of-shear (Gorinova et al. 2019). This prevalent deformation formed under amphibolite-facies conditions during earliest Late Cretaceous (100–90 Ma), syn-metamorphic, northwestward thrusting of the Variscan high-grade metamorphic rocks over the Kabul Unit (Gorinova 2020). The fabric is sealed by the 60–58 Ma old Kalin pluton (Zagorchev et al. 2014; Gorinova et al. 2019; Fig. 2). Later, between 58 and 48 Ma, the Kabul Unit was thrust over the Malyovitsa Unit along the Dodov Vrah Shear Zone (Gorinova 2020, Fig. 2). This shear zone hosts deformed diorites to gabbro–diorite bodies with a protolith age of ca. 76 Ma (U–Pb zircon ages, Gorinova et al. 2019).

North Rhodopean Unit

Most previous authors attribute this unit to the Upper Rhodopean Terrane (e.g. Burg 2012; Froitzheim et al. 2014; Schmid et al. 2020, Fig. 1). However, Sarov et al. (2006) included it within the newly established Thrace Lithotectonic Unit, together with the Sakar Unit of the Sakar–Strandja Zone (Fig. 1).

The North Rhodopean Unit consists of biotite, muscovite and two-mica gneisses, marbles and amphibolites, all affected by upper greenschist to low-grade amphibolite-facies metamorphism related to the formation of generally subhorizontal northwest–southeast striking foliation bearing a subhorizontal lineation (Naydenov et al. 2008). Naydenov et al. (2009) report U–Pb zircon mean ages of between 162.9 ± 3.6 and 155.9 ± 4.4 Ma for the youngest deformed magmatic rocks, suggesting an Alpine age for the main metamorphic event in this unit. A Late Jurassic–Early Cretaceous age of the metamorphism is further constrained by Late Cretaceous age granitoids that intrude into the gneisses (Fig. 2, Naydenov et al. 2009). The North Rhodopean Unit is separated from the Chepino Unit by the North Rhodopean Detachment (Fig. 2).

Variscan high-grade metamorphic units

Variscan high-grade metamorphic rocks are reported in the study area both above and below the North Rhodopean Detachment. The rocks west of the Kabul Unit, which were previously attributed to the Ograzhden metamorphic complex (Sarov et al. 2011b, Fig. 2), were later described as the Polich Unit (Gorinova et al. 2019) of the Upper Allochthon of the Rhodope Metamorphic Complex (e.g. Froitzheim et al. 2014). The Variscan rocks below the North Rhodopean Detachment consist of migmatized biotite and two-mica gneisses that host bodies of metagabbros (Sarov et al. 2011b). Their lower boundary is the amphibolite-facies Bistritsa Shear Zone, along which the Polich Unit was thrust over the Kabul Unit (Fig. 2). Sense-of-shear criteria indicate top-to-the-northeast (Sarov et al. 2011b) or northwest-directed tectonic transport (Gorinova et al. 2019).

The high-grade metamorphic rocks situated north of the Dzherman and Cherni Iskar rivers, above the North Rhodopean Detachment were equally attributed to the Ograzhden (Sarov et al. 2011a) and later to the Sredna Gora units (Gorinova et al. 2019, Fig. 2). They are made up of migmatized biotite and two-mica gneisses hosting bodies of metagabbros and lenses of serpentinized ultrabasites. Late Ordovician protolith ages are reported for the migmatized gneisses (U–Pb zircon ages between 454 and 446 Ma; Peytcheva et al. 2009). There are no studies for the metamorphic evolution of these rocks. However, similar metamorphic rocks farther north in the basement of the Sredna Gora Zone are intruded by undeformed Carboniferous to Permian granites, suggesting a Variscan age of the regional migmatisation and metamorphism (Carrigan et al. 2005, 2006; Gerdjikov et al. 2010).

North Rhodopean Extensional System

Shipkova and Ivanov (2000) were the first to describe a Cenozoic detachment fault (the Dzherman Detachment) that borders the Rila Mountains to the west and northwest and underlies the late Eocene–Oligocene Padala basin (Fig. 2, Cernjavska 2000). Later, Sarov et al. (2011a, b) describe another detachment located between Sapareva Banya and Govedartsi (Fig. 2) named the Lakatitsa Detachment. Further east, in the area of Sestrimo (Fig. 2), the brittle–ductile shear zone separating the Chepino Unit from North Rhodopean Unit is termed the North Rhodopean Detachment (Naydenov et al. 2008). More recently, Gorinova et al. (2019) describe the whole extensional structure that borders the northwestern Rila Mountains as the North Rila Detachment, up to where it is cut by the brittle, high-angle, Saparevo normal fault along the northwestern slope of the Rila Mountains (Fig. 2).

In the study area, Gorinova et al. (2019) describe a lower grade, north-dipping mylonitic foliation overprinting the older fabric along the North Rila Detachment. The generally shallow-dipping fabric of this zone outcrops in a large area

along the western bank of the Dzherman River and also on the mountain slopes south of Govedartsi (Fig. 2). The kinematic indicators show a consistent top-to-the-north–northwest sense-of-shear and the age of displacement is latest Eocene to early Oligocene (Gorinova et al. 2019). Large parts of the detachment zone were offset by normal faults formed during later extensional tectonics.

In this study, the extensional shear zones together with the brittle to brittle–ductile North Rhodopean Detachment, developed along the northern slopes of the Rila Mountains, are referred to as the North Rhodopean Extensional System, following Gerdjikov et al. (2006).

Rila–West Rhodope Batholith (RWRB)

The batholith is built of a succession of at least four granitic magmatic pulses intruded during the Maastrichtian to the late Eocene time (Valkov et al. 1989; von Quadt and Peytcheva 2005; Peytcheva et al. 2007). The first phase consists of granodioritic and quartz–dioritic rocks that form the largest body in the area, called the Belmeken body emplaced at 70.77 ± 0.09 Ma (U–Pb zircon age) (Valkov et al. 1989; Peytcheva et al. 2007; Fig. 2). These granodiorites, which have a calc-alkaline affinity with a mixed (mantle-crustal) magma source, were formed in a subduction-related setting (Kamenov et al. 1999).

The most widespread lithologies within the batholith are the medium- to coarse-grained biotite granites intruded during the second phase. In the study area, this phase is represented by the Musala body and a small part of the Western Rhodope body in the eastern part of the area, as well as the muscovite–biotite Shpanyovitsa body (Fig. 2). There are no geochronological data for the Musala body, but the Shpanyovitsa granite has a U–Pb zircon age of 39.39 ± 0.21 Ma (Peytcheva et al. 2007). The third phase consists of several small, fine-grained granite to plagiogranite bodies, such as the Chavcha (Fig. 2). The granites of the second and third phase have a high K calc-alkaline affinity with isotopic compositions diagnostic of a mixed mantle-crustal origin. However, their crustal component is considerably higher in comparison to the Late Cretaceous granodiorites of the first phase (Kamenov et al. 1999). Therefore, the granites of the second and third phase are considered to have formed in late- to post-collisional tectonic settings (Kamenov et al. 1999). Stocks and veins of isotropic aplitoid and pegmatoid granites form the fourth phase (Fig. 2). The emplacement of the RWRB led to the formation of the north–northwest to south–southeast elongated Rila–West Rhodope dome (e.g. Ivanov 2017), where the granitoids form the core of the dome, with a rim of high-grade metamorphic rocks (Fig. 1).

Structural studies along the North Rhodopean Extensional System

As defined in this paper, the North Rhodopean Extensional System (NRES) comprises the brittle–ductile to brittle low-angle North Rhodopean Detachment that is underlain by a relatively narrow ductile mylonitic shear zone and a wide protomylonitic zone. Below, is a description of the different elements of the extensional system that outcrop along the northern slopes of the Rila Mountains between the towns of Dupnitsa and Sestrimo (Fig. 2). This system was previously traced as far east as the area of Krichim (Gerdjikov and Gautier 2006) (Fig. 1), but its relationship with the detachment system of the Central Rhodope Metamorphic Complex remains unclear (Kounov et al. 2020).

Brittle North Rhodopean Detachment

Unfortunately, exposures of this detachment zone in the study area are limited, because it is either buried below lower Oligocene sedimentary rocks and the North Rhodopean Thrust or offset by Miocene–Quaternary normal faults (Fig. 2). Sometimes its existence is only deduced by the presence of brecciated and silicified zones in the footwall.

Sestrimo area

South to southeast of Sestrimo the brittle detachment can be followed (Fig. 3), along the contact between the Chepino and North Rhodopean units. In the rest of the area, it is either buried below the North Rhodopean Thrust or is partially offset by the Miocene–Quaternary Sestrimo normal fault (Valkova and Spiridonov 1979) (Fig. 3). The detachment zone is best studied along the Sestrimska River valley, where the uppermost part of the footwall and tectonites of the detachment zone crop out (Figs. 3, 5a). The fault zone consists of 3 to 5 m thick, black ultra-cataclasites that overlay ultramylonitic gneisses, marbles and pegmatites of the Chepino Unit (Fig. 5a). The direct contact with the hanging wall, comprising strongly faulted gneisses, amphibolites, schists and marbles of the North Rhodopean Unit, is covered by colluvium.

Govedartsi area

In the Govedartsi area, the detachment zone is partly reactivated and/or offset by the Govedartsi normal fault (Fig. 4). The zone is easily mappable by following the lithologically contrasting boundary between the leucocratic orthogneisses of the Preka Reka Unit in the footwall, and the dark Variscan high-grade gneisses and amphibolites in the hanging

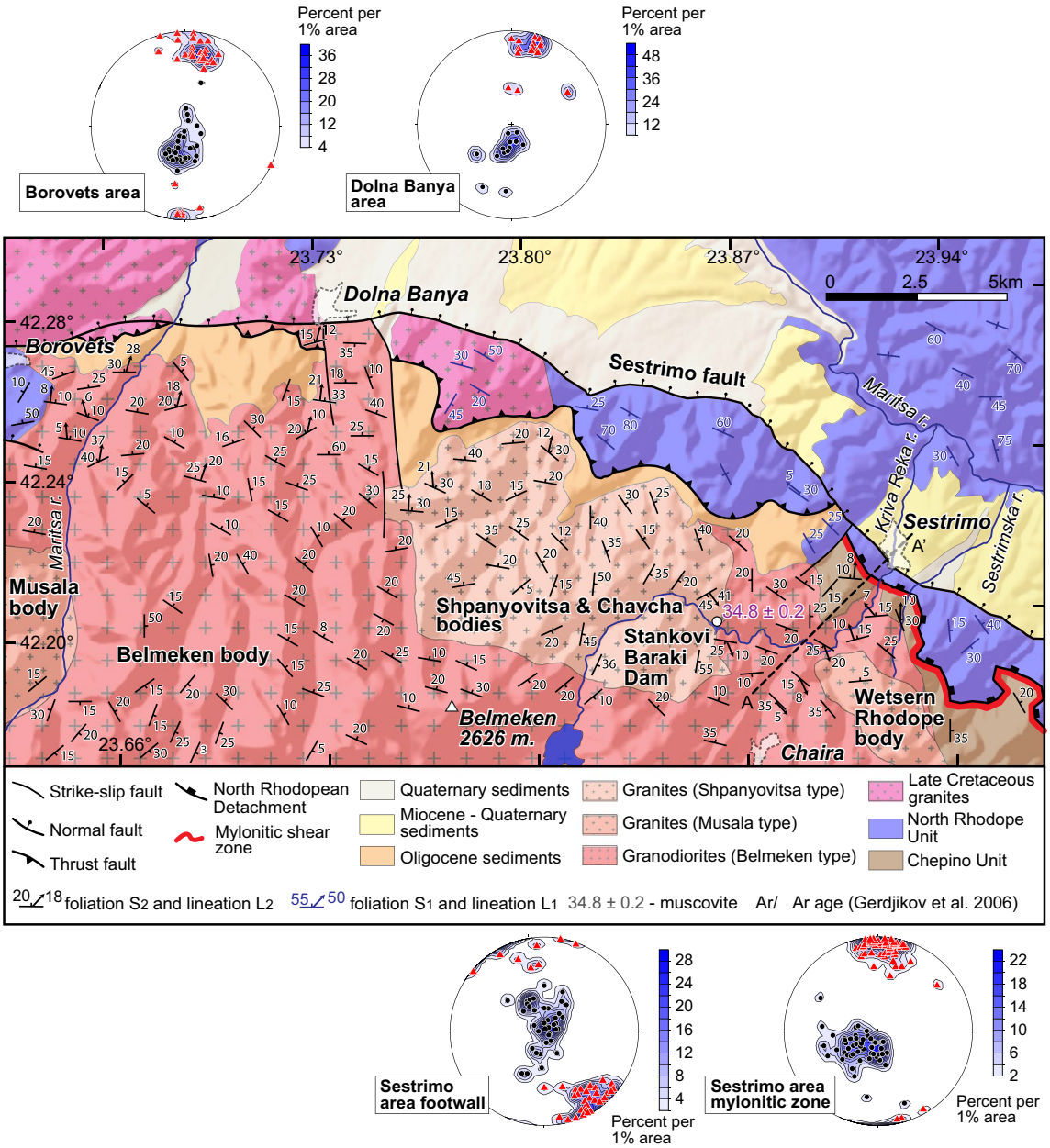

Fig. 3 Geological map of the area between Borovets and Sestrimo (modified after 1:50,000 geological maps of Bulgaria) with lower hemisphere equal-area plots of structural elements related to the Cenozoic extension. Solid black circles indicate S_2 foliation poles and the closed red triangles the L_2 stretching lineation. Lithological key as in Fig. 2. Line AA′ is the section in Fig. 5

wall (Fig. 4). Brecciated and silicified rocks from the uppermost structural parts of the footwall mark the zone at several localities in the vicinity of Govedartsi. Along the road to Mechit hut (Fig. 4), black ultra-cataclasites crop out above the brecciated and silicified orthogneisses (Fig. 5b).

Dzherman River valley

A wide brittle fault zone that separates the Malyovitsa Unit from the Variscan high-grade metamorphic rocks along the Dzherman River valley has previously been described as a thrust (Marinova and Zagorchev 1991) and a detachment zone (Lakatitsa Detachment of Sarov et al. 2011a, or North Rila Detachment of Gorinova et al. (2019). The brittle zone often has a steep dip due to its reactivation and tilting along the Dzherman normal fault (Figs. 4, 5c). To the north, the fault zone is cut by the Miocene–Quaternary Saparevo normal fault, whereas to the south, it is covered by Oligocene and Quaternary sedimentary rocks (Marinova and Zagorchev 1991, Fig. 4).

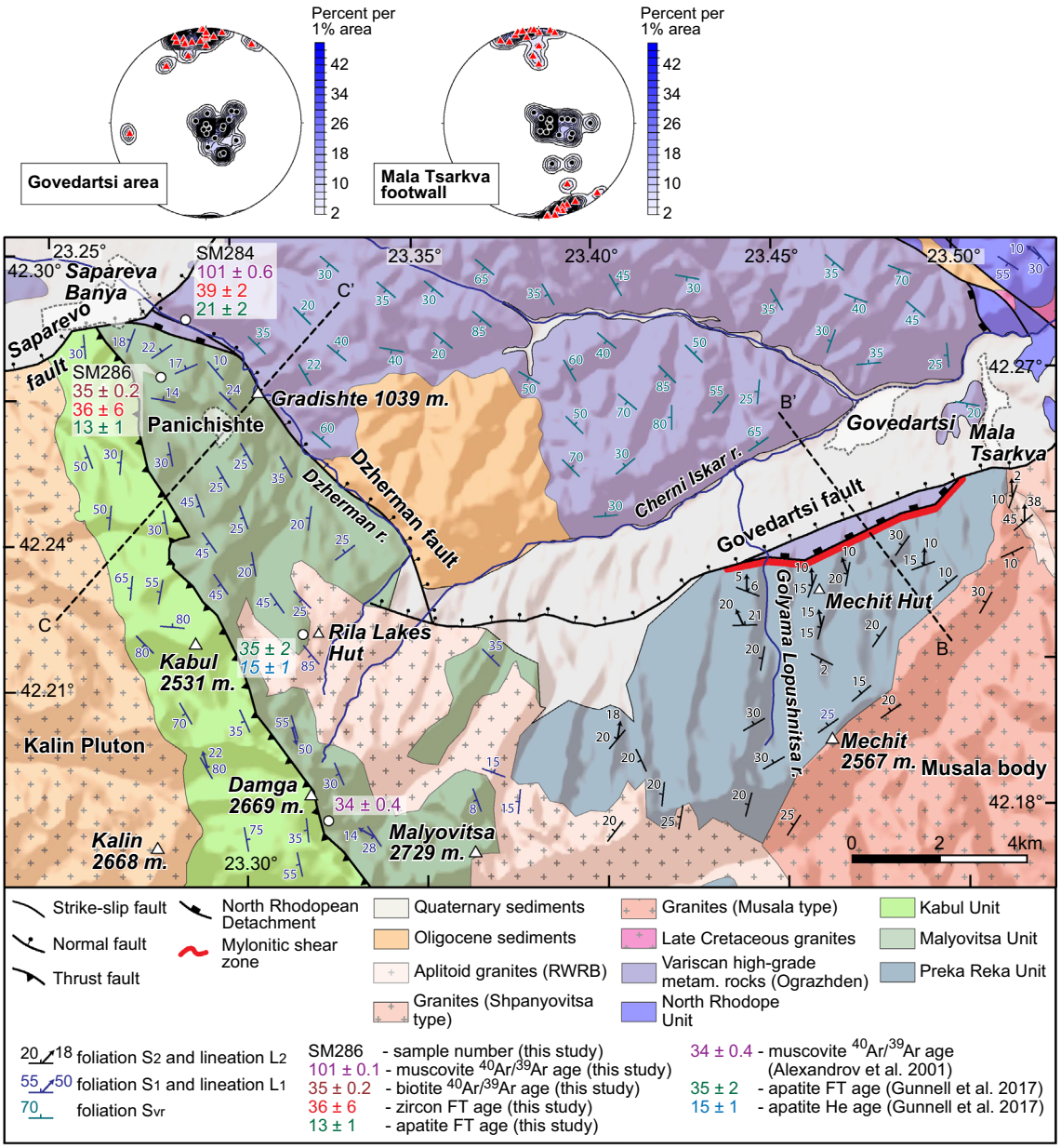

Fig. 4 Geological map of the area between Sapareva Banya and Govedartsi (modified after 1:50,000 geological maps of Bulgaria) with location and ages of analysed samples and previously published data together with lower hemisphere equal-area plots of structural elements related to the Cenozoic extension. Solid black circles indicate S_2 foliation poles and the closed red triangles indicate L_2 stretching lineation. Lithological key as in Fig. 2. Lines BB′ and CC′ are the sections in Fig. 5

In the area of the Dzherman River, the Malyovitsa gneisses in the footwall of the detachment are intruded by voluminous leucocratic granitic dykes and pegmatites. All these rocks are strongly cataclastically deformed along a ~ 50 m thick zone (Fig. 5c). The zone is capped by several metres thick grey gauge and/or tectonic breccias. Quaternary slope deposits cover the contact with the Variscan migmatites in the hanging wall of the detachment. An almost complete section across the detachment zone was observed to the northeast of the Gradishte Peak, where the deeply incised Dzherman River cuts through the zone (Figs. 4 and 5c). Here, the footwall comprises alternating biotite gneisses, various schists, amphibolites and rare marble layers intruded by pegmatitic dykes. These rocks display only the older penetrative schistosity S_1 that is conformable to the detachment zone (Fig. 4). There is no evidence of intensive ductile deformation that could be related to the extension. The uppermost ca. 10 m of the footwall are affected by strong brecciation,

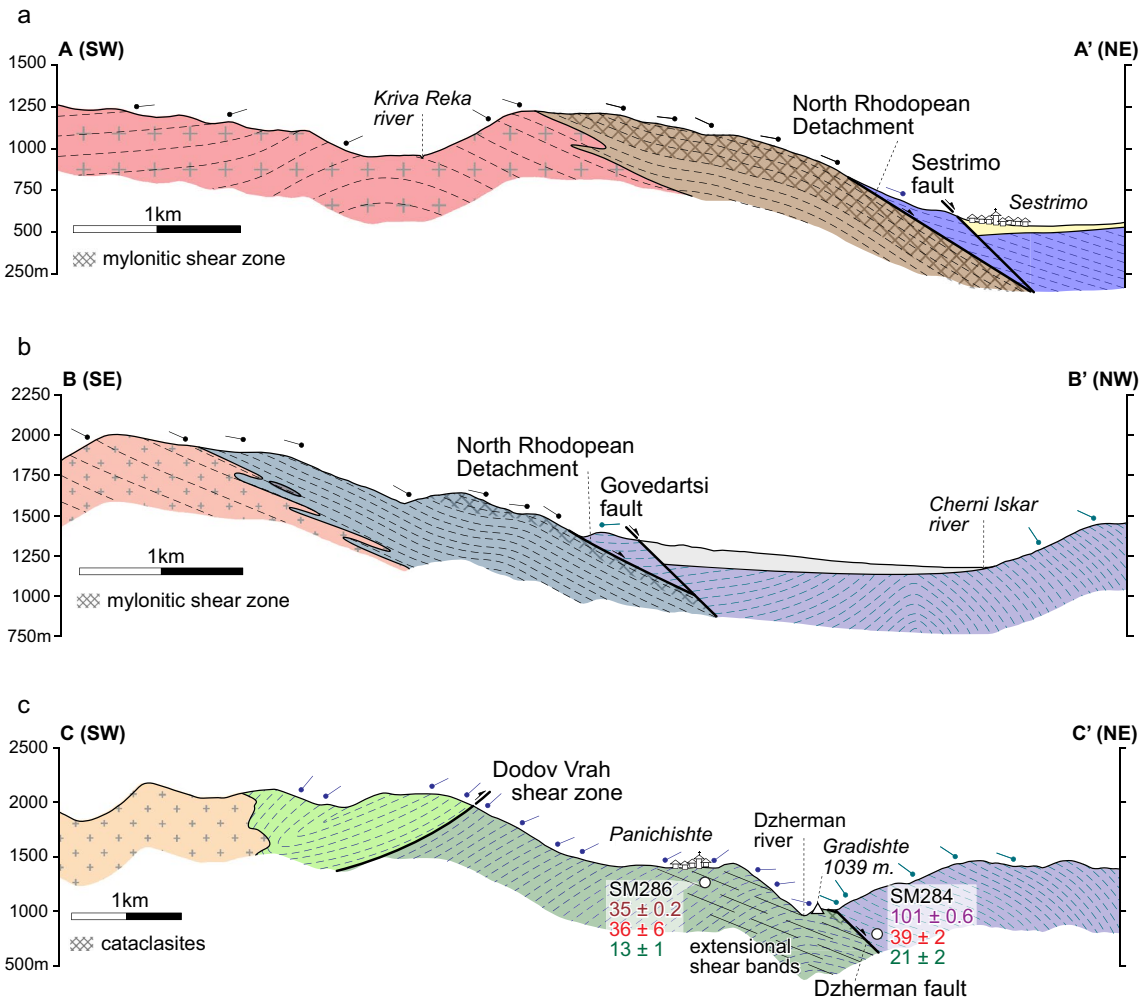

Fig. 5 Sections AA′, BB′ and CC′ with the projected geochronological ages from this study. Lithological key as in Fig. 2. For location, see Fig. 3 for traces AA′ and Fig. 4 for traces BB' and CC′. Vertical scale equal to the horizontal

silicification and propylitization, and cut by numerous millimetres to centimetres thick ultra-cataclasite zones and faults. The ultra-cataclasite zones generally dip steeply (50–60°) to the east–northeast and often form an anastomosing network. With the exception of some mechanically competent, low-strain lenses (represented mainly by pegmatites and coarse gneisses), the brecciated rocks display a weakly developed S_2 cataclastic foliation that strikes parallel to the contact. Extensional, top-to-the-northeast kinematics can be deduced by the geometric relationship between the shallower S_2 cataclastic foliation and a steeper set of northeast-dipping brittle shear zones (Fig. 6a).

Mylonitic shear zone

A high-strain zone of upper greenschist- to lower amphibolite-facies metamorphic (medium-grade) mylonites (450–600 °C, Passchier and Trouw 2005; Trouw et al. 2009), exposed below the detachment, is best observed at two particular localities in the Sestrimo and Govedartsi areas (Fig. 2). In places, the medium-grade mylonites are overprinted by greenschist-facies metamorphic (low-grade) mylonites and ultramylonites (300–400 °C, Passchier and Trouw 2005; Trouw et al. 2009). Our observations show that, although differing in relative temperature, both the medium-grade mylonites and the low-grade ultramylonites show a top-to-the-north sense-of-shear and are therefore probably a result of the same deformation event. The relative temperature difference between the mylonites occurs because, as the footwall of the detachment moved upward during crustal extension, the medium-grade mylonites that formed at depth were displaced to progressively shallower levels, undergoing retrograde deformation and strain localisation causing cataclasis and brecciation (e.g. Lister and Davis 1989). Therefore, we attribute the penetrative ductile fabric associated with the

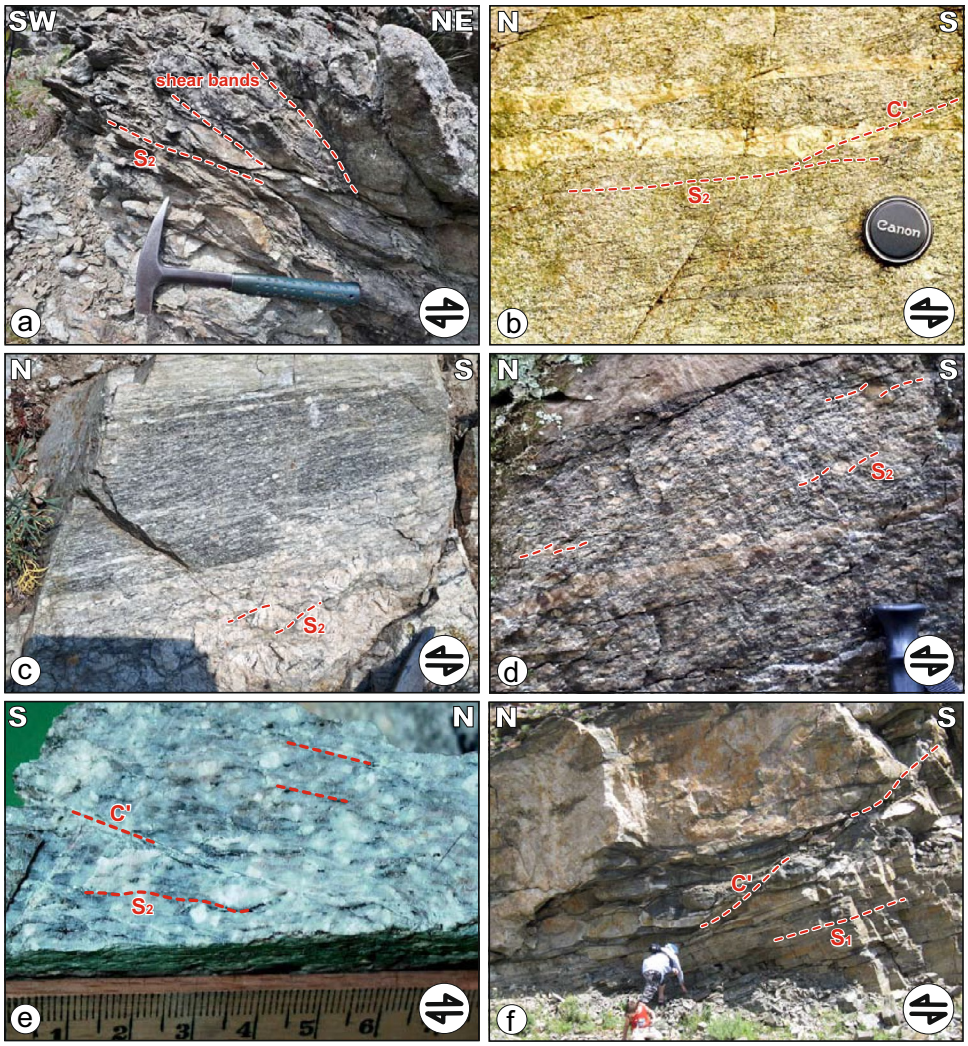

Fig. 6 Structural features of the Rhodope Metamorphic Complex. **a** Extensional, northeast-dipping, brittle shear zones cutting shallower cataclastic foliation S_2 showing top-to-the-northeast sense-of-shear in the Malyovitsa Unit, near Gradishte Peak (N42.26975, E23.30720); **b** densely spaced C' shear bands within the ultramylonites showing top-to-the-north sense-of-shear in the Chepino Unit gneisses, Sestrimo area (N42.19752, E23.86340); **c** asymmetric, sigma-type K-feldspar porphyroclasts showing top-to-the-north sense-of-shear in the Chepino Unit gneisses, Sestrimo area (N42.20547, E23.91760); **d** asymmetric K-feldspar porphyroclasts systems showing top-to-the-north sense-of-shear in the Preka Reka orthogneisses, Govedartsi area (N42.23085, E23.44563); **e** C' shear bands indicate top-to-the-north sense-of-shear in the Shpanyovitsa granites, Sestrimo area (N42.25572, E23.72570); **f** northeast-dipping extensional C' shear bands cutting shallower dipping old foliation S_1 and voluminous granitic dykes showing top-to-the-north sense-of-shear in Malyovitsa metamorphic rocks, Sapareva Banya–Panichishte area (N42.27363, E23.27985)

top-to-the-north sense-of-shear to crustal extension. The absence of a medium-grade mylonitic zone in other parts of the study area may be due to offset by a later brittle detachment and subsequent normal faulting, or because it was never exhumed (e.g. the area of the Dzherman River valley and southwest of Sapareva Banya, Fig. 2).

Sestrimo area

In the Sestrimo area, the mylonitic shear zone is about 100 to 250 m wide (Fig. 5a). It developed on the dark biotite gneisses, amphibolites and migmatites of the Chepino Unit, which are intruded by a variety of dykes, including fine-grained biotite granites, leucogranites and pegmatites, most probably related to the Shpanyovitsa granites (Peytcheva et al. 2007). Most of the granitic dykes are concordant to the mylonitic foliation S_2 in the host rocks and have a pervasive solid-state fabric that in places grades from C/S mylonites to ultramylonites. Lower strains observed in the granitic dykes in comparison to the metamorphic rocks of the Chepino Unit could be due to their higher mechanical competency and/or syn-tectonic emplacement. South of Sestrimo, Von Quadt and Peytcheva (2005) report zircon and monazite single grain U–Pb ages of between 43 and 41 Ma from a deformed granitic vein intruded in the Chepino Unit. The lower contact of the shear zone outcrops along the road from Sestrimo to Chaira (Fig. 3), where it exhibits a sharp shear gradient between the mylonitic host rocks of the Chepino Unit and protomylonitic granodiorites of the RWRB. Previously this shear zone has been described as a part of the Yadenitsa-Grashovo brittle–ductile extensional shear zone, which follows, in places, the contact between the Belmeken granodiorites and the West Rhodopean granites (Naydenov et al. 2008, Fig. 3).

The mylonitic foliation S_2 is principally defined by biotite, muscovite, quartz ribbons and stretched leucosomes and has a generally shallow dip (10–25°) towards the northeast (Fig. 3). However, the orientation of the foliation

does vary due to post-mylonitic faulting. Newly formed black hornblende and biotite along the foliation planes, as well as feldspar core and mantle structures and quartz recrystallisation by a subgrain rotation and grain boundary migration mechanisms indicate upper greenschist- to lower amphibolite-facies deformation conditions (ca. 450–600 °C, Stipp et al. 2002; Passchier and Trouw 2005, Fig. 7b, c). Grain-size reduction and the formation of low-grade ultramylonitic levels are observed within the shear zone as well as densely spaced C' shear bands, which indicate strain localization during the exhumation (Dimov and Georgiev 2000, Figs. 6b and 7a). Isoclinally folded, centimetre-thick quartz–feldspar leucosome bands are often reduced to rootless hinges. Their axes are subparallel to the stretching lineation and axial planes are concordant to the mylonitic foliation S_2. These folds formed during the folding of an earlier migmatitic fabric S_1. The mylonites display a prominent north–south trending stretching lineation L_2 that is commonly observed on S_2 foliation and the shear bands (Fig. 3). The lineation is defined by elongated quartz and quartz–feldspar mineral aggregates, the alignment of hornblende crystals and clots of white mica. Kinematic indicators within the medium-grade mylonites and the low-grade ultramylonites include asymmetric, sigma and delta-type K-feldspar porphyroclasts, asymmetric boudinage and C' shear bands (Fig. 6b and c). All these features indicate a general top-to-the-north sense-of-shear, which corroborates previously published data (Dimov and Georgiev 2000; Gerdjikov et al. 2006). Within the foliated granitic dykes, a pervasive C/S fabric also shows a top-to-the-north sense-of-shear.

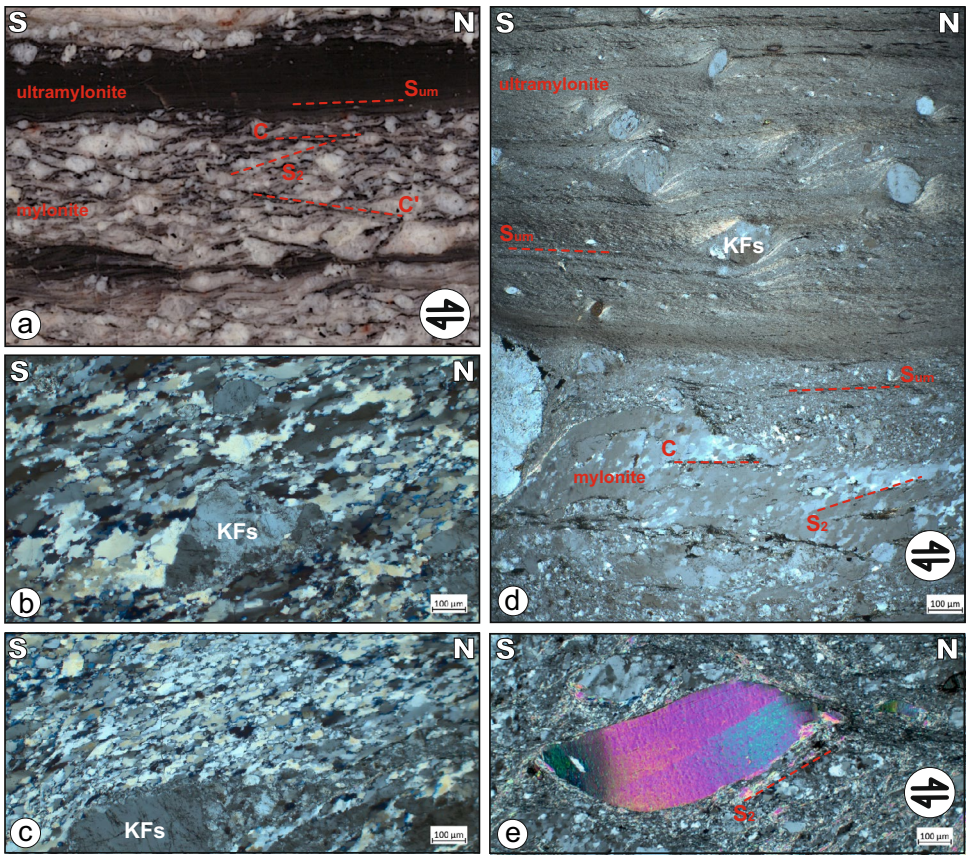

Fig. 7 Mylonitised Belmeken granodiorites from the area of Stankovi Baraki Dam (42.192639 N, 23.885038 E) at the footwall of the North Rhodopean Detachment (Fig. 3). **a** Hand-sized specimen of mylonitic and ultramylonitic granodiorite with polished surface. C/S fabrics together with C'-type shear bands indicating top-to-the-north sense-of-shear. Due to the high-strain rate the ultramylonitic foliation S_{um} is parallelized to the C-type shear bands. **b**, **c** Partially recrystallised K-feldspar porphyroclasts (KFs) within a matrix of dynamically recrystallised by a subgrain rotation and grain boundary migration mechanism quartz indicating upper greenschist to lower amphibolite-facies (medium-grade) deformation conditions (ca. 450–600 °C, Stipp et al. 2002; Passchier and Trouw 2005). **d** Ultramylonites formed mostly by bulging recrystallization indicating lower greenschist-facies temperature conditions between 300 and 400 °C (Stipp et al. 2002; Passchier and Trouw 2005) overprinting an older upper greenschist to lower amphibolite-facies medium-grade mylonitic C/S fabric both indicating top-to-the-north sense-of-shear. Delta- and sigma-type K-feldspar porphyroclasts (KFs) indicate top-to-the-north sense-of-shear. **g** Mica fish indicating top-to-the-north sense-of-shear

Govedartsi area

The mylonitic shear zone in the Preka Reka Unit orthogneisses is ~ 50 m thick (Figs. 4, 5b). Most outcrops are situated along steep river valleys, because much of the area is covered by Quaternary glacial and alluvial–colluvial deposits. An almost complete section of the shear zone outcrops along the Golyama Lopushnitsa River (Figs. 4). Here, 2–3 m thick, gently north–northwest-dipping ultramylonites are visible (Fig. 5b) immediately below the brittle detachment. The ultramylonitic rocks are massive, homogenous and lack a macroscopically observable foliation fabric. They consist of a black-green, chlorite-rich matrix that hosts K-feldspar porphyroclasts with diameters of ~ 1 cm and rarely, larger pegmatitic clasts.

Mylonitic orthogneisses are present structurally below the ultramylonitic zone (Fig. 5b). In fact, the low-grade ultramylonitic zone described above develops on this earlier fabric. The most common lithology is white to pink biotite orthogneiss with up to 2 cm large K-feldspar porphyroclasts (Fig. 6d). More rarely, banded biotite orthogneisses are seen, probably formed at the expense of equigranular granite, which consist of quartz ribbons alternating with a fine-grained matrix containing feldspar porphyroclasts and biotite. Leucogranite and pegmatite dykes concordant to the foliation are also common (Fig. 6d). Most of them are intensely deformed, although some still exhibit a weakly developed foliation. The foliation S_2 in the mylonites dips shallowly (5–20°) to the north–northwest (Fig. 4) and is defined by polycrystalline quartz ribbons recrystallized tails around K-feldspar porphyroclasts and biotite flakes. The stretching lineation L_2 generally plunges towards the north and is defined by aligned mineral aggregates, elongated K-feldspar porphyroclasts and quartz rods (Fig. 4). The foliation planes are often cut by steeper shear bands that are up to 1–2 cm wide and characterised by a pronounced grain-size reduction. The shear bands and asymmetric K-feldspar porphyroclasts indicate a top-to-the-north sense-of-shear (Fig. 6d).

Deformation in the footwall of the NRES below the mylonitic shear zone

Intense ductile deformation related to extensional tectonics is observed in large parts of the footwall below the mylonitic shear zone. The main interpretation challenge is distinguishing younger extension-related fabric from older one formed during Mesozoic to Paleocene crustal shortening. Direct relationships between both fabrics are not observed because they are subparallel. This parallelism could be due to relatively coaxial principal strain axes for both tectonic events or rotation of the older contractional structures. Consequently, the actual extent and character of the extensional deformation can only be evaluated by observations on the Late Cretaceous to late Eocene granites of the RWRB (von Quadt and Peytcheva 2005; Peytcheva et al. 2007; Figs. 3 and 4). Since these granites postdate the main Mesozoic metamorphism in the Rhodopean complex, their deformation can be exclusively attributed to the Cenozoic extension.

Two domains with a differing character of ductile deformation are distinguished in the footwall of the NRES. In the eastern and central parts of the Rila Mountains, east of the Dzherman River valley (Fig. 2), the NRES is better developed and an almost full section of the system is observed, including the brittle low-angle detachment fault and the mylonitic shear zone below it (Fig. 2). The omission of the detachment fault and reduction of the mylonitic shear zones at certain places is due to later thrusting and normal faulting (Figs. 2, 3 and 4). On the other hand, the deformation in the footwall is less intense along the northwest slope of Rila Mountains, west of the Dzherman River valley (Fig. 2) where the upper greenschist- to lower amphibolite-facies mylonitic shear zone, if formed at depth, was never exhumed to the surface. Accordingly, the extension-related deformation in the footwall of the system will be discussed in two separate domains-Eastern and Western.

Eastern domain

In the Eastern domain, to the east of Dzherman River valley, the footwall of the NRES mainly comprises composite RWRB (Fig. 2). Most of the Belmeken granodiorites display a moderate to intensely developed solid-state foliation S_2, whilst lineations L_2 are less frequent (Fig. 3). The strain intensity varies and protomylonites predominate. The foliation below the mylonitic zone has a shallow dip to the northwest, north or east, whilst in the southwestern part of the study area it has a shallow dip to the southwest (Fig. 3). The Shpanyovitsa and Chavcha bodies, which crop out along the slope of the Rila Mountains to the west of Sestrimo (Figs. 2 and 3), show solid-state deformation. Protomylonites are developed in the northwestern part of the granites, as well as along its northern margin. Locally they grade into mylonitic and ultramylonitic zones that have a thickness of tens of centimetres. In the western part of the granite, the foliation S_2 has a shallow dip to the north–northeast (Fig. 3) and is marked by aligned quartz aggregates and micas. The stretching lineation L_2 plunges towards the north and north–northeast (Fig. 3). C' shear bands indicate a top-to-the-north sense-of-shear (Fig. 6e).

The contact between the Shpanyovitsa granite and the Belmeken granodiorites is well exposed along the road between Sestrimo and Stankovi Baraki Dam (Fig. 3). Here, the granites of the Shpanyovitsa body display a weakly developed southeast-dipping foliation S_2, whereas a prominent strain gradient is observed towards the contact with

the Belmeken granodiorites. The gradient marks a transition from weakly foliated granite to protomylonites and C/S mylonites (Gerdjikov et al. 2006). Locally the C/S mylonites are overprinted by low-grade ultramylonites. Ultramylonites formed mostly by bulging recrystallization, indicating lower greenschist-facies temperature conditions between 300 and 400 °C (Stipp et al. 2002; Passchier and Trouw 2005; Fig. 7 d). The Belmeken granodiorites are intruded by a large number of leucocratic dykes that often display a solid-state deformational fabric. Numerous shear sense criteria, such as C/S fabric, mica fishes, sigma- and delta-type K-feldspar porphyroclasts indicate a top-to-the-northwest to north–northwest sense-of-shear (Fig. 7 d, e). The Belmeken granodiorites are cross-cut by a younger and voluminous pulse of coarse-grained biotite granites (Musala body, Valkov et al. 1989, Fig. 2). Field data from the section to the south of Mala Tsarkva (Fig. 4) document a zone of intense solid-state deformation that is several tens of meters thick. The foliation dipping to the north–northwest bears a down-dip stretching lineation (Fig. 4). Shear bands indicate a top-to-the-north–northwest sense-of-shear. Mesocratic, ultramylonitic zones up to 20 cm thick are also observed.

In the westernmost part of the Eastern domain, the Govedartsi area, below the mylonitic zone of the NRES, the foliation in the Jurassic orthogneisses of the Preka Reka Unit dips to the northwest to west (Fig. 4). The direct relationship between this foliation and the extensional mylonitic zone is not observed in this area, and thus it remains unclear if the deformation is related to the extension or the earlier contraction. The shear sense indicators are also not observed. Therefore, only steeply dipping shear bands that intersect the foliation planes and indicate a general top-to-the-north sense-of-shear, are considered to be related to Cenozoic extensional phase.

Western domain

The Western domain extends from the Dzherman River valley to the town of Dupnitsa, along the northwestern slope of the Rila Mountains. Here, the footwall of the NRES consists of amphibolite-facies metamorphic rocks of the Malyovitsa and Kabul units, as well as Variscan high-grade metamorphic rocks (Sarov et al. 2011a; Gorinova et al. 2019; Figs. 2 and 4). The medium-grade mylonitic shear zone is missing in this domain, and the extensional deformation is expressed by low-grade mylonites and extensional shear bands.

In the Sapareva Banya–Panichishte area, the older contraction-related foliation S_1 between the Kalin pluton and the Dzherman River valley generally trends north–northwest to south–southeast and dips in both directions (Fig. 4). First, Dimov and Damianova (1996) and later Gorinova et al. (2019) describe a major top-southeast ductile shear zone, which accommodates thrusting of the Kabul Unit onto the Malyovitsa Unit (Fig. 4). In both units, the foliation planes have a north–northwest to south–southeast-trending stretching lineation L_1 (Fig. 4). Shear sense criteria show a top-to-the-southeast sense-of-shear (Gorinova et al. 2019).

The highest confidence observations of extensional deformation in this area are made between Sapareva Banya and Panichishte (Fig. 4). Here, voluminous granitic melts were intruded into the metamorphic rocks, in a range from fine-grained biotite granites to leucocratic granites and pegmatites (Fig. 6f). Granitic dykes and veins are concordant with, or cross-cut the penetrative foliation S_1 that dips to north–northwest (Fig. 4). A large number of cross-cutting dykes of mostly biotite granites are devoid of any apparent solid-state overprint, whereas some of the concordant dykes display a fine foliation marked by the alignment of micas and stretched quartz. Northeast-dipping extensional C' shear bands that cut a shallow dipping, S1 foliation and granitic dykes, indicate a top-to-the-north sense-of-shear (Fig. 6f). A generally north-dipping stretching lineation, formed by stretched quartz and white mica flakes, is observed on the shear planes.

In the area west of Kalin pluton, Shipkova and Ivanov (2000) describe a brittle detachment fault (Dzherman Detachment) underlain by a ductile mylonitic zone along the northwest slope of the Rila Mountains. Later, Gorinova et al. (2019) confirm the existence of greenschist-facies metamorphic extensional mylonites in this area, where the brittle deformation superimposed on the mylonites is attributed to the movements along the younger Saparevo normal fault (Fig. 2). However, new field observations made for this study do not identify a brittle detachment in the area. Instead, the old contraction-related foliation is cut by steeper shear bands and centimetre-thick, low-grade shear zones indicating a top-to-the-north sense-of-shear, similar to the fabric observed in the Sapareva Banya–Panichishte area. A noteworthy difference in the area west of the Kalin pluton is the lack of any voluminous intrusions of granitic and pegmatitic dykes and veins.

Thermochronology

The $^{40}Ar/^{39}Ar$ and fission-track analytical procedures and methodologies are described in Online Appendix A. The geographic location of the analysed samples and the results are presented in Fig. 4 and Tables 1 and 2, whilst relevant $^{40}Ar/^{39}Ar$ age spectra are shown in Fig. 8. Use the term plateau age is according to the recommendation of Schaen et al. (2021), such that (i) a plateau must have at least 5 consecutive steps that constitute $\geq 50\%$ of the total ^{39}Ar released by step-heating, (ii) the plateau steps must not form a positive or negative slope, and (iii) the $^{40}Ar/^{36}Ar$ atmospheric value must be 298.56 ± 0.31 (Lee et al. 2006). The $^{40}Ar/^{39}Ar$ date

Table 1 Results of $^{40}Ar/^{39}Ar$ thermochronology

Heating step	$^{40}Ar/^{39}Ar$	$\pm 1\sigma$	$^{37}Ar/^{39}Ar$	$\pm 1\sigma$	$^{36}Ar/^{39}Ar$	$\pm 1\sigma$	$^{40}Ar^*/^{39}Ar_k$	$\pm 1\sigma$	^{40}Ar (mol)	$^{40}Ar^*$ (%)	$^{39}Ar_k$ (%)	Age (Ma)	$\pm 2\sigma$ (Ma)	K/Ca	$\pm 2\sigma$
SM286-3 biotite, $J = 0.0041268 \pm 0.0000125$					Plateau age 34.90 ± 0.15 Ma										
1	9.52969	0.01976	0.02373	0.00126	0.01971	0.00030	3.706660	0.08779	1.874E−15	38.90	2.69	27.39	1.29	18.12	1.92
2	5.88042	0.01187	0.01843	0.00068	0.00409	0.00014	4.671659	0.04193	2.343E−15	79.44	5.44	34.45	0.61	23.33	1.73
3	5.45347	0.01098	0.01074	0.00073	0.00290	0.00008	4.595258	0.02614	2.603E−15	84.26	6.52	33.89	0.38	40.02	5.47
4	5.22388	0.01052	0.01100	0.00050	0.00170	0.00007	4.721232	0.02327	3.761E−15	90.38	9.84	34.81	0.34	39.10	3.55
5	5.10602	0.01028	0.01029	0.00047	0.00125	0.00005	4.736838	0.01686	4.667E−15	92.77	12.49	34.93	0.25	41.78	3.84
6	5.06312	0.01016	0.00923	0.00034	0.00112	0.00003	4.731006	0.01356	6.456E−15	93.44	17.42	34.88	0.20	46.58	3.39
7	5.00673	0.01003	0.01174	0.00036	0.00092	0.00003	4.733945	0.01211	6.312E−15	94.55	17.23	34.90	0.18	36.62	2.24
8	4.92589	0.00989	0.01240	0.00038	0.00065	0.00003	4.733506	0.01244	5.265E−15	96.09	14.60	34.90	0.18	34.67	2.14
9	4.88598	0.00984	0.01313	0.00064	0.00038	0.00007	4.772469	0.02197	3.085E−15	97.68	8.63	35.19	0.32	32.76	3.20
10	4.84946	0.00983	0.01181	0.00097	0.00069	0.00013	4.644716	0.04079	1.823E−15	95.78	5.14	34.25	0.60	36.40	5.96
SM284-1 muscovite, $J = 0.0041413 \pm 0.0000125$					Plateau Age 100.79 ± 0.55 Ma										
1	31.14170	0.09593	0.01491	0.00998	0.06984	0.00150	10.504789	0.44025	1.116E−15	33.73	0.94	76.82	6.30	n/a	n/a
2	16.16220	0.03523	0.00000	0.00335	0.00745	0.00034	13.958795	0.10393	2.538E−15	86.37	4.14	101.39	1.47	n/a	n/a
3	15.09862	0.03083	0.00052	0.00127	0.00334	0.00018	14.110840	0.06112	4.663E−15	93.46	8.14	102.46	0.86	n/a	n/a
4	14.45244	0.02931	0.00233	0.00142	0.00260	0.00016	13.684577	0.05382	5.789E−15	94.69	10.56	99.45	0.76	n/a	n/a
5	14.62633	0.02969	0.00000	0.00119	0.00284	0.00018	13.786191	0.06013	5.841E−15	94.26	10.52	100.17	0.85	n/a	n/a
6	14.52631	0.02924	0.00000	0.00009	0.00159	0.00013	14.055988	0.04721	7.863E−15	96.76	14.27	102.07	0.67	n/a	n/a
7	14.47317	0.02985	0.00000	0.00017	0.00189	0.00015	13.913158	0.05250	4.942E−15	96.13	9.00	101.06	0.74	n/a	n/a
8	14.37738	0.03027	0.00051	0.00024	0.00242	0.00021	13.660219	0.06856	3.668E−15	95.01	6.72	99.28	0.97	n/a	n/a
9	14.42186	0.02935	0.00000	0.00024	0.00178	0.00020	13.893954	0.06566	4.173E−15	96.34	7.63	100.93	0.93	n/a	n/a
10	14.31508	0.02924	0.00000	0.00010	0.00153	0.00010	13.861309	0.04019	4.792E−15	96.83	8.82	100.70	0.57	n/a	n/a
11	14.25734	0.02924	0.00032	0.00015	0.00121	0.00016	13.898538	0.05564	4.205E−15	97.48	7.77	100.96	0.79	n/a	n/a
12	14.49169	0.02945	0.00000	0.00009	0.00192	0.00011	13.922956	0.04301	6.315E−15	96.08	11.48	101.13	0.61	n/a	n/a

Mass discrimination 0.983 ± 0.051

Data are corrected for blanks, interfering nucleogenic reactions and decay of 37Ar and 39Ar

Irradiated for 15 h at Oregon State University, TRIGA, CLICIT, $^{39}Ar/^{37}Ar$ 6.73E−4, $^{36}Ar/^{37}Ar$ 2.64E−4, $^{40}Ar/^{39}Ar$ 1.01E−3, $^{38}Ar/^{39}Ar$ 1.138E−2

Steps highlighted with bold text are included in the calculation of the weighted mean age and the plateau age

Samples heated with a IR-CO2 laser for 30 s, with 5 min cleaning with a ST101 and AP10 getter in a stainless steel extraction line

Data collected with an Argus mass spectrometer. Multi collection with 1E11Ω Faraday (^{40}Ar) and 1E12Ω Faradays (^{39}Ar. ^{38}Ar. ^{37}Ar. ^{36}Ar)

Procedure identical to that described in Villagomez and Spikings (2013)

^{40}Ar—radiogenic argon isotope

$^{39}Ar_K$—Potassium-derived isotope of argon

Table 2 Apatite (AP) and zircon (ZR) fission-track results

	Sample number	Min.	Latitude/ longitude	Alt. M	Lithology	Strat. division	Num. gr.	ρd (Nd) $\times 10^6$ cm^{-2}	ρs (Ns) $\times 10^6$ cm^{-2}	ρi (Ni) $\times 10^6$ cm^{-2}	P (χ^2) (%)	U. conc. (ppm)	Central age (± 1σ) Ma	MTL(± 1σ) µm	Std. dev. (*N*) µm	Dpar. µm
1	SM284	AP	N42.28534/ E23.28712	778	Migmatite	Ograzhden unit	23	1.243(7076)	0.137(265)	1.319(2554)	11	12 ± 9	21.4 ± 1.5	14.99 ± 0.95	1.65(3)	1.87
		ZR					23	0.485(3585)	6.219(1396)	4.740(1064)	62	312 ± 62	38.6 ± 1.9			
2	SM286	AP	N42.27363/ E23.27985	1238	Biotite schist and leucocratic granite	Malyovitsa unit	20	1.228(7076)	0.148(165)	2.269(2532)	83	21 ± 7	13.3 ± 1.1	14.58 ± 0.55	0.78(2)	2.01
		ZR					3	0.479(3585)	8.470(93)	8.922(76)	80	458 ± 115	35.6 ± 5.6			

All ages are reported as central ages (Galbraith and Laslett 1993)

ρd induced track density, *ρs*, *ρi* densities of spontaneous and induced tracks, respectively, $P(\chi^2)$ is the probability of failing the χ^2-test, *Dpar* track pit diameter of a sample. *MTL* mean track length; *n* number of lengths measured

is only considered to be robust if the plateau age overlaps with the inverse isochron date.

^{40}Ar/^{39}Ar data

A migmatite sample (SM284) from Variscan high-grade metamorphic rocks is taken from a pristine roadside outcrop east of Sapareva Banya (Fig. 4). The foliation, defined by flattened quartz–feldspar aggregates, white mica and biotite, dips westward at shallow angle. An aliquot of muscovite grains between 300 and 250 µm in size were hand-picked for ^{40}Ar/^{39}Ar analysis. The initial heating step yields a relatively young date of 76.82 ± 6.30 Ma, although the subsequent 5 heating steps yield a plateau date of 100.79 ± 0.55 Ma, and an inverse isochron date of 100.31 ± 2.98 Ma (MSWD = 2.39) (Fig. 8a). A biotite schist sample (SM286) from the Malyovitsa Unit is taken from a roadside outcrop southeast of Sapareva Banya (Fig. 4). Foliation in the schists dips to the north–northwest. A biotite concentrate was hand-picked from the fraction coarser than 160 µm. The initial (lower temperature) heating steps yield dates that span between 27.39 ± 1.29 and 33.89 ± 0.38 Ma, whilst seven subsequent heating steps, corresponding to ~ 80% of the ^{39}Ar released, define a plateau date of 34.90 ± 0.15 Ma, and an inverse isochron date of 34.961 ± 0.36 Ma (MSWD = 1.37) (Fig. 8b).

Fission-track data

The low number of apatite grains, combined with their low uranium content and high number of defects, did not allow measurement of sufficient horizontal confined track lengths to obtain useful track length statistics, inhibiting numerical thermal modelling (Rahn and Seward 2000). The migmatite sample (SM284) from the Variscan high-grade metamorphic rocks yielded a zircon FT Central age of 38.6 ± 1.9 Ma with P(χ^2) of 62 and an apatite FT Central age of 21.4 ± 1.5 Ma with P(χ^2) of 11 (Fig. 4 and Table 2). Three measured confined tracks in apatite give a mean track length of 14.99 ± 0.95 µm, and a standard deviation of 1.65 µm (Table 2). Biotite schist sample (SM286) from the Malyovitsa Unit yielded a zircon FT Central age of 35.6 ± 5.6 Ma with P(χ^2) of 80 and an apatite Central age of 13.3 ± 1.1 Ma with P(χ^2) of 83 (Fig. 4 and Table 2). Two measured confined tracks in apatite give a mean track length of 14.58 ± 0.55 µm, and a standard deviation of 0.78 µm (Table 2).

Interpretation and discussion

The low number of analysed samples and the lack of numerical thermal modelling of the apatite FT data limit constraints on the cooling histories of the rocks exposed in the study

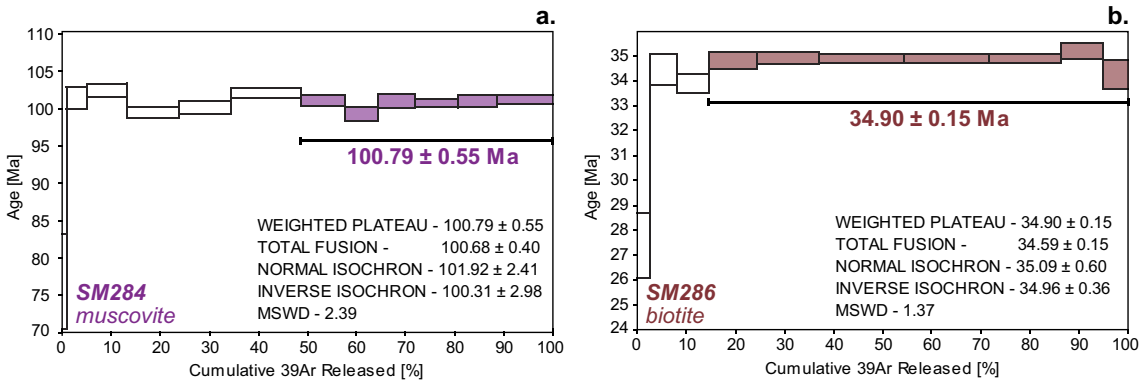

Fig. 8 Relevant $^{40}Ar/^{39}Ar$ date spectra for sample from the Variscan high-grade metamorphic rocks (SM284) and Malyovitsa Unit (SM286). All uncertainties are $\pm 2\sigma$. Plateau dates are defined according to Schaen et al. (2021)

area. On the other hand, the combination of the $^{40}Ar/^{39}Ar$ and fission-track data from the same rocks in combination with previously published ages (Figs. 3 and 4) permits some conclusions to be made regarding the time and rates of exhumation. The detailed structural analysis and data in this study provide a link between the exhumation histories and structural evolution of the area. Finally, temporal correlations with tectonic phases identified in neighbouring areas strengthen the thermal history and tectonic conclusions.

Late Early to early Late Cretaceous evolution

Assuming the Ar isotope compositions of the muscovite are not modified by recrystallisation/fluid flow, the muscovite $^{40}Ar/^{39}Ar$ plateau date of the migmatised orthogneiss sample (SM284) from the Variscan high-grade metamorphic rocks suggest it reached a temperature between 440 and 400 °C (Harrison et al. 2009) at 101 ± 0.6 Ma (Fig. 4). This age corresponds to a late Early Cretaceous shortening event that resulted in north–westward thrusting of the Variscan high-grade metamorphic rocks onto the Kabul Unit along the Bistritsa Shear Zone (Gorinova et al. 2019, Fig. 2). If the sampled Variscan metamorphic rocks to the northeast of Dzherman valley is part of this thrust sheet, the burial depth of these rocks was at least between 10 and 14 km at the end of the Early Cretaceous (assuming a typical for orogenic belts geothermal gradient of 30 and 40 °C/km). Consequently, this overburden has been eroded during the mid-Cretaceous age shortening and/or a subsequent extension. Indeed, it is difficult to evaluate whether the muscovite plateau date of 101 ± 0.6 Ma of the migmatite (SM284) is related to cooling due to erosion synchronous with thrust sheet emplacement or post-contractional cooling. Certainly, these events are not related to the formation of a new ductile fabric in the studied part of the Variscan metamorphic rocks, because the only observed fabric is the migmatitic layering overprinted by high-grade foliation S_{VR} (Fig. 4), which is cut by undeformed Carboniferous to Permian granites farther north (e.g. Carrigan et al. 2005).

North of the study area, Velichkova et al. (2004) report muscovite and biotite $^{40}Ar/^{39}Ar$ ages between 105 and 99 Ma related to an Alpine metamorphic overprint associated with ductile deformation along discrete strike-slip shear zones in the Variscan high-grade metamorphic rocks of the Sredna Gora Zone (Fig. 1). On the other hand, thermochronological studies from the neighbouring Kraishte Zone (Kounov et al. 2010) and farther west, in central parts of the Serbo-Macedonian Massif (Antić et al. 2016, Fig. 1), suggest the Albian to Cenomanian (112–90 Ma) is a period of regional extension. In Sredna Gora Zone to the north (Fig. 1), calc-alkaline magmatic activity is coeval with this extension and the formation of intra-arc volcano-sedimentary basins, or possibly one large basin with several depocenters filled with Cenomanian to Maastrichtian deposits (e.g. Dabovski et al. 2009; Ivanov 2017). Therefore, it is possible the northwest Rhodope was also under post-contractional extension at that time, like some other parts of the Balkanides.

Eocene–early Oligocene extension and activity along the North Rhodopean Extensional System

Time and rate of cooling and exhumation

The zircon FT age of 39 ± 2 Ma from the migmatite sample (SM284) in the hanging wall of the North Rhodopean Extensional System (Ograzhden Unit, Fig. 4) corresponds to the time of emplacement of the Shpanyovitsa granitic phase of the RWRB (U–Pb zircon age of 39 ± 0.2 Ma; Fig. 2) (Peytcheva et al. 2007) and, therefore, could be related to an increase in the thermal gradient in the area. On the other hand, the biotite schist sample (SM286) from the footwall of the extensional system (Malyovitsa Unit, Fig. 4) yields $^{40}Ar/^{39}Ar$ biotite (34.90 ± 0.15 Ma) and zircon FT ages (35.6 ± 5.6 Ma, Fig. 4) that are statistically indistinguishable

from each other. However, no further interpretation of the FT zircon age is attempted because the date is obtained from track density measurements only based on three grains (Table 2) and is thus not considered a statistically robust result.

Elsewhere around the study area, Gunnell et al. (2017) report an apatite FT age of 35 ± 1.8 Ma for a diorite located close to the Rila Lakes hut, at an elevation c. 1000 m above the biotite schist sample (SM286) (Fig. 4). Considering the altitude difference and closure temperatures of both mineral systems, a geothermal gradient of ~ 200 °C/km at ~ 35 Ma is deduced (Ar-in-biotite and FT-apatite; mean effective closure temperature of ~ 310 °C for Ar–biotite, Harrison et al. 1985; 110 ± 10 °C for apatite FT, Gleadow and Duddy 1981). Such a high geothermal gradient seems unrealistic and would be regionally anomalous, because there are no reports of magmatic intrusions of similar age in the area having created such a temperature difference. Consequently, a more likely interpretation is a high exhumation rate of ~ 5 km/Ma during the cooling of the whole ~ 1 km thickness of rocks between the two samples (using a geothermal gradient of 40 °C/km suggested by Gunnell et al. 2017 for eastern Rila during the Paleogene). An even higher estimate of exhumation rate in the area is derived from an $^{40}Ar/^{39}Ar$ phlogopite plateau age of 34.2 ± 0.4 Ma obtained from a granitic pegmatite vein located ~ 1 km southeast of Damga Peak (Alexandrov et al. 2001) (Fig. 4). The dated sample is taken from a similar elevation in the vicinity of the diorite sample Gunnell et al. (2017) report (Fig. 4). Considering the overlapping ages of both samples and the closure temperatures of Ar in white mica (~ 440–400 °C, Harrison et al. 2009) and the FT-apatite mineral systems (cited above), a cooling rate of ~ 330–290 °C/Ma are estimated. Again, using the assumption of a geothermal gradient of 40 °C/km (Gunnell et al. 2017), this corresponds to more than 7 km/Ma of exhumation at ~ 35–34 Ma. It is important to note that such high cooling rates are incompatible with simple erosion-driven, subaerial denudation of the Rila Mountains during the Cenozoic, as suggested by Gunnell et al. (2017). In this case, tectonically driven denudation in this area seems a more probable explanation. The possibility that the phlogopite $^{40}Ar/^{39}Ar$ age corresponds to the time a pegmatite vein forms, as suggested by Alexandrov et al. (2001), or consequent fluid flow may also be excluded. Late, syn-kinematic granitic pegmatitic and aplitic veins that intrude the Malyovitsa Unit have ages between 47 and 51 Ma (U–Pb zircon ages, Gorinova et al. 2019), whereas the youngest granitic pulse in the RWRB occurs at 39.39 ± 0.21 Ma (U–Pb zircon age, Peytcheva et al. 2007). Therefore, we attribute the very fast exhumation of these rocks at about 35–34 Ma to fault activity along the North Rhodopean Extensional System (Fig. 9a). Fast cooling between 38 and 35 Ma are also recorded in the eastern parts of the Rila Mountains, based on the results of thermal modelling of apatite FT data (Gunnell et al. 2017). A muscovite $^{40}Ar/^{39}Ar$ plateau age of 34.8 ± 0.2 Ma was also reported from the deformed Eocene granite in the eastern Rila Mountains near the Stankovi Baraki Dam's wall (Gerdjikov et al. 2006, Fig. 3).

Recently, some authors advocate that fast cooling episodes constrained by thermochronological data could be related to thermal relaxation, postdating a major orogenic event rather than to substantial direct exhumation (e.g. Braun 2016; Wolff et al. 2020). However, this model is discarded as a possibility that explains the exhumation in the study area because the time of the cooling stage estimated by the new data is coeval with both massive erosion and the deposition of a substantial amount of late Eocene age (Priabonian, 37.7–33.9 Ma, Cohen et al. 2022) sediments (Fig. 1, e.g. Zagorchev et al. 1989, see also the discussion below). Significant exhumation is also corroborated by the fact the 39-Ma-old Shpanyovitsa granite is exposed by early Oligocene (33.9–27.8 Ma, Cohen et al. 2022) and reburied under sediments of the Lakatitsa and Kostenets basins (Naydenov et al. 2008, Figs. 2 and 9b). The sedimentary rocks in the Padala Basin are also of early Oligocene age (Figs. 2 and 9b, Cernjavska 2000). In addition, the substantial amount of exhumation is evidenced by the fact that the upper greenschist- to lower amphibolite-facies metamorphic (medium-grade) mylonites were overprinted by greenschist-facies metamorphic (low-grade) ultramylonites in the footwall of the North Rhodopean Detachment (Fig. 7d). This retrograde overprint and strain localisation in these rocks took place during ascent from deeper to progressively shallower crustal levels as exhumation progressed.

Differential exhumation along the NRES

Structural observations along the NRES suggest the amount of exhumation varies along the zone. The footwall in the eastern part of the system, where the structurally deeper part of the Rhodope Metamorphic Complex is exposed, the Chepino Unit (e.g. Burg 2012), experienced the maximum exhumation (Fig. 2). Logically, in this part of the system (Sestrimo area, Fig. 3), the thickest mylonitic zone is developed below the brittle detachment, where early medium-grade mylonites are later overprinted by low-grade mylonites and ultramylonites. Unlike the eastern domain, in the western domain (west of the Dzherman River valley, Fig. 2), there are no exposures of extensional medium-grade mylonites and deformation along the NRES is accommodated by low-grade mylonites and ductile–brittle to brittle deformation. If medium-grade mylonites did form at depth, they have never been exhumed to the surface. Accordingly, in this part of the NRES, only the uppermost parts of the

Rhodope Metamorphic Complex are exhumed to the surface (the Malyovutsa and Kabul units) together with its Variscan metamorphic tectonic cover (e.g. Burg 2012; Gorinova et al. 2019; Fig. 2). In the area of the Padala basin, the relationship between the North Rhodopean Detachment and the ductile mylonitic shear zone (Shipkova and Ivanov 2000, Fig. 2) is still uncertain. The thermochronological methods in use in this study do not record the differential exhumation along the NRES because the footwall rocks are exhumed from depths with temperatures in excess of ~ 300–400 °C, which is higher than the closure temperature of the applied thermochronological methods.

Syn-extensional sedimentation

In the study area, Eocene age extension was either not accompanied by deposition of syn-tectonic sediments or the sedimentary rocks of this age are not preserved due to subsequent erosion. However, sediments derived from the substantial extension and denudation in the north Rila could possibly be deposited farther east in the Upper Thrace basin (Fig. 1), where Bartonian to Priabonian sedimentary rocks are penetrated in boreholes (e.g. Popov et al. 2015). Upper Eocene–lower Oligocene sediments are deposited in the hanging wall of the North Rhodopean Detachment farther east in the Izvor–Peshtera Basin (Fig. 1, Sarov et al. 2008a, b). Later, the detachment is sealed by the Oligocene volcanic rocks, the Bratsigovo–Dospat ignimbrites (U–Pb age of 31.63 ± 0.40 Ma, Marchev et al. 2022), which erupted into this basin. Late Eocene (Priabonian) sedimentary rocks associated with extension also outcrop in many other parts of the Rhodope Metamorphic Complex, south and southeast of the study area (Fig. 1, e.g. Cernjavska 1977; Boyanov and Goranov 2001), as well as in Kraishte Zone, adjacent to the northwest Rila Mountains (Fig. 1, Zagorchev et al. 1989). This widespread sedimentation is cited by many authors as evidence for the time of onset of regional extensional tectonics (e.g. Pleuger et al. 2011; Kounov et al. 2004, 2020). The sedimentation in most areas continues into the early Oligocene, which suggests the cessation of activity along the North Rhodopean Detachment (Fig. 9b) is not necessarily coincident with the end of crustal extension in the area.

Correlations with neighbouring areas

The end of the Eocene and the beginning of the Oligocene is a time of substantial crustal extension, affecting the whole southern part of the Balkan Peninsula (e.g. Burchfiel et al. 2008; Kounov et al. 2018), which is characterised by core complexes formation and low-angle normal faulting across all parts of the Rhodope Metamorphic Complex (Dinter and Royden 1993; Krohe and Mposkos 2002; Bonev et al. 2006; Brun and Sokoutis 2007; Kounov et al. 2015, 2020; Georgiev et al. 2010, 2016), and the Kraishte area (e.g. Kounov et al. 2004; Antić et al. 2016). For example, the Central Rhodope Metamorphic Complex experiences rapid cooling between 37 and 33 Ma, from temperatures > 650 °C down to ~ 60 °C, associated with partial melting and formation of multiple generations of detachment faults (e.g. Kounov et al. 2020). The Eocene extensional event is also identified in the neighbouring Balkan Fold-Thrust Belt (Fig. 1), where it started in the middle Eocene (~ 44 Ma, Kounov et al. 2018). Recently, Balkanska et al. (2022) reported two stages of post-orogenic middle Eocene to Oligocene extension (45–42 and 34–28 Ma) from the central parts of the Sredna Gora Zone (Fig. 1) crystalline basement, which is ~ 50 km northeast of the studied area.

Late Oligocene–early Miocene heating event

Consideration of Miocene apatite FT ages from both sides of the North Rhodopean Detachment (13.3 ± 1.1 and 21.4 ± 1.5 Ma, Fig. 4) suggests reheating reset the FT ages of these rocks after being at, or close to, the surface in the early Oligocene, as suggested by their proximity to the transgressive contact with sedimentary rocks of the same age (Naydenov et al. 2008, Fig. 4). Based on their apatite (U–Th)/He and FT data, Danišík et al. (2014) define a late Oligocene–early Miocene heating event related to top-to-the-south thrusting of the North Rhodopean Unit over the metamorphic rocks and granites cropping out today in the Rila Mountains. The present-day structure attributed to this event is the North Rhodopean Thrust, which extends along the northern boundary of the Rila–Rhodope Massif, and along which the rocks of the North Rhodopean Unit and Late Cretaceous granites are thrust over lower Oligocene sedimentary rocks (e.g. Naydenov et al. 2008, Fig. 2). However, the tectonic settings and amount of displacement on this thrust are still disputed. Zagorchev (1992) suggests ~ 1 to 5 km displacement along this structure, whereas Naydenov et al. (2008) suggest it is a transpressional domain of the dextral strike-slip Maritsa Fault Zone, which formed during the latest brittle stage of the fault zone tectonic evolution (Figs. 1 and 9c). Localised occurrences of late Oligocene to early Miocene contractional structures related to a short-lived period of regional shortening are reported from Thrace Basin in Greece (e.g. Kilias et al. 2013), as well as several other places across the Balkan Peninsula (e.g. Dumurdzanov et al. 2005; Burchfiel et al. 2008). This tectonic event is associated with an early Miocene depositional hiatus observed in most basins of the southern Balkan Peninsula (e.g. Zagorchev 1996; Dumurdzanov et al. 2005).

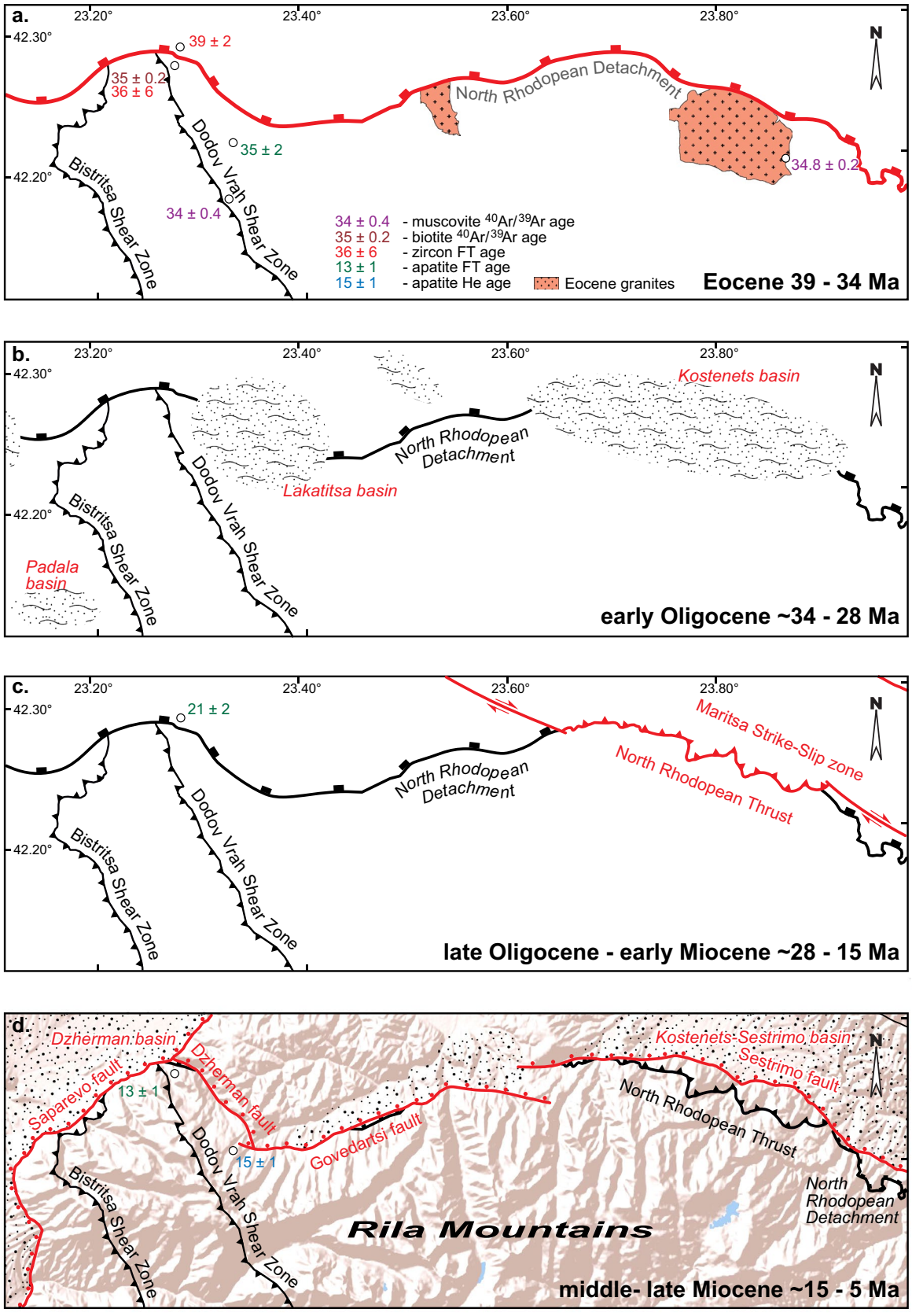

Fig. 9 Schematic model for the tectonic evolution of the study area. The area presented in the figure corresponds to this given in Fig. 2

Middle–late Miocene extension

The apatite FT ages of the samples from the Malyovitsa Unit (13.3 ± 1.1 Ma; SM286) and the Variscan high-grade metamorphic rocks (21.4 ± 1.5, Ma; SM284) suggest cooling of the analysed rocks in the study area to below 110 ± 10 °C must have taken place in the Miocene (Fig. 4). The brittle–ductile low-angle North Rhodopean Detachment was no longer active at this time as it was already sutured by lower Oligocene sedimentary rocks. However, some differential movement along the contact between these two units must still have occurred, given their different apatite FT ages. Today, normal faults border most of the northern slope of the Rila Mountains and the Saparevo and Sestrimo faults are the largest amongst them (Fig. 2). Displacement along these faults is related to the development of the Miocene to Quaternary Dzherman and Kostenets–Sestrimo basins (Sarov et al. 2011a; Naydenov et al. 2008; Figs. 2, 9d). Some displacement during this time may also occur along the Govedartsi normal fault, which is probably connected to the Saparevo normal fault along the Dzherman fault, which acts as a relay ramp breaching fault (e.g. Fossen and Rotevatn 2016, Fig. 9d). The apatite FT age from the uplifted footwall block of this fault system, suggests the onset of movement along the faults, and the subsequent growth of the basins probably started close to 13 Ma, or after. The diorite sample taken close to the Rila Lakes hut by Gunnell et al. (2017) yields a (U–Th)/He apatite age of 15 ± 1 Ma (Fig. 4), which further suggests some cooling and exhumation occurred during 15–13 Ma. An early to middle Miocene (22–13 Ma) tectonically induced pulse of denudation is suggested by Gunnell et al. (2017) based on apatite (U–Th)/He ages from the Rila Mountains. Middle–late Miocene cooling of the Rila basement complex was also reported by Danišík et al. (2014), based on combined apatite (U–Th)/He and FT data. The middle to late Miocene (~ 12–6 Ma) is also characterised by exhumation along brittle normal faults cutting the Strymon Valley Detachment and the formation of syntectonic sedimentary basins west of the Pirin Mountains, and farther south in the Southern Rhodope Metamorphic Complex (Kounov et al. 2015; Stübner et al. 2016; Fig. 1). These steeply dipping brittle normal faults led to rift-flank uplift and the formation of high topography subject to rapid erosion (Stübner et al. 2016). A similar scenario could be suggested also for our study area where possible high relief formed during the Miocene has partially persisted until today.

Multistage extension evolutionary model

The long and complicated evolution of the syn- to post-orogenic extension and exhumation along the orogenic belts can only be thoroughly revealed by a combination of appropriate thermochronological methods and detailed structural analysis. The coupling of new and previously published $^{40}Ar/^{39}Ar$, fission-track and (U–Th)/He data, together with structural studies of the ductile to brittle deformation of rocks from the northwest part of the Rhodope Metamorphic Complex, allow reconstruction of the exhumation history of these rocks from 600 to less than 110 °C during the Cenozoic extension. The first phase of exhumation in the RMC during the Eocene (39–35 Ma), accommodated by the North Rhodopean Detachment, is related to back-arc extension triggered by slab rollback and Aegean trench retreat (e.g. Brun and Faccenna 2008; Forster and Lister 2009; Kounov et al. 2020). This forms classical extensional detachment zone along which amphibolite-faces metamorphic rocks have been continuously exhumed through greenschist-facies to finally brittle deformation conditions (e.g. Lister and Davis 1989). A decreasing amount of exhumation along the more than 150 km east–west trending detachment zone (from Krichim to Dupnitsa areas, Fig. 1) is observed from west to the east. It may tentatively be suggested that farther west the zone is connected with the Middle Rhodopean Detachment (Fig. 1), which has exhumed even deeper crustal rocks that have experienced anatexis during the extension (e.g. Kounov et al. 2020).

After a phase of mostly strike-slip and thrust tectonics, the second middle–late Miocene extensional stage (15–13 Ma) is associated with the formation of high-angle brittle normal faults. It is difficult to say if these faults are listric and connect with a sole detachment at depth. If yes, such a structure is not exhumed, although the extension continues even during the Quaternary, indicated by the continuous sedimentation in the extensional basins surrounding the Rila Mountains (Fig. 2, Zagorchev 1992). Unlike the first stage, related to the Aegean back-arc extension, the second might just result from a westward extrusion of Anatolian plate along the North Anatolian Fault (NAF, Fig. 1), which pulls the southern Balkan lithosphere slowly to the south, causing regional north–south extension (e.g. Burchfiel et al. 2008). A lack of trench rollback related hot mantle material underlying the Rhodope Metamorphic Complex did not allow melt to spread and trigger stretching in the lower crust which was characteristic of the Eocene extension. Consequently, the middle to late Miocene extension is accommodated only by movement along high-angle brittle normal faults whereas middle to lower crustal rocks are not exhumed. Crustal extension continues even today in the area of Rila Mountains, as suggested by present-day seismicity data indicating active displacement is ongoing along some faults that bound the mountain chain (e.g. Kotzev et al. 2006). The highest present-day topography is in the Rila and Pirin Mountains in comparison to the rest of the Rhodope massif, which could be related to some post-glacial rebound

and/or isostatic equilibrium because up to 50 km thick crust underlie this area (Boykova 1999).

Conclusions

The combination of previously published and new thermochronological data ($^{40}Ar/^{39}Ar$, fission-track and (U–Th)/He) coupled with detailed structural studies reveal a multistage tectonically induced exhumation of the northwestern Rhodope Metamorphic Complex in the northern Rila Mountains. The following stages are constrained for the period of evolution between the late Mesozoic and the Cenozoic in the study area:

1. New $^{40}Ar/^{39}Ar$ data constrain cooling of the Variscan high-grade metamorphic basement to temperature below 440–400 °C at about 101 ± 0.6 Ma caused by either erosion of the emplacing thrust sheet, or post-contractional extension and denudation.
2. An Eocene age pulse of increased cooling between 39 and 35 Ma is induced by exhumation along the North Rhodopean Extensional System. During this progressive exhumation, in the footwall of the North Rhodopean Detachment upper greenschist- to lower amphibolite-facies metamorphic mylonites were successively overprinted by greenschist-facies metamorphic mylonites and finally by brittle–ductile to brittle cataclasis and brecciation. The amount of exhumation along the NRES increases from the west towards the east, where deeper parts of the Rhodope Metamorphic Complex are exhumed. The extensional system became inactive in the early Oligocene and is sealed by transgressive terrigenous deposits. However, extension did not entirely stops at the transgression as shown by the continuing development of Eocene to Oligocene sedimentary basins within the Rhodope Metamorphic Complex as well as in neighbouring areas.
3. Both the new and previously published fission-track and (U–Th)/He analysis provide evidence of a heating event during the early Miocene in the study area, which is probably related to strike-slip and thrust tectonics.
4. The middle–late Miocene extensional stage is associated with movements along brittle, steeply dipping normal faults which control the formation of extensional sedimentary basins in their hanging walls. This extension continues even in the Quaternary, shown by the continuous sedimentation in the basins bordering the Rila Mountains and also led to the development of high local relief in the Rila and Pirin Mountains.

Cenozoic multistage extension in the northwestern Rhodope Metamorphic Complex is governed by northward subduction of the Tethys Ocean beneath Eurasia and the consequent reorganisation of plate boundaries along its margin. If Eocene extension is related to rollback and continuous retreat of the subducted slab, the later middle–late Miocene extension is triggered by the westward movement of the Anatolian plate, which induces north–south extension north of the North Anatolian Fault Zone. An initial phase of subduction-related regional extension is associated with the formation of large detachment zones responsible for the exhumation of middle to lower crustal rocks. A subsequent later phase of regional extension is accommodated by high-angle normal faults, which are responsible for the formation of continental basins in their hanging walls and high topographic relief in their footwalls.

Acknowledgements This study was partially financed through the Swiss National Science Foundation grants NEW1532 and NUW1518. IG field mapping of the Miocene–Quaternary fault network benefited from funding from National Science Programme "Environmental Protection and Reduction of Risks of Adverse Events and Natural Disasters", approved by the Resolution of the Council of Ministers No 577/17.08.2018 and supported by the Ministry of Education and Science (MES) of Bulgaria (Agreement No D01-230/06.12.2018). We thank Pierre Gautier for his help in the field and the fruitful discussions. We appreciate the reviews of the topic editor Niko Froitzheim and the editor-in-chief Ulrich Riller as well as of Nikolay Bonev and one anonymous reviewer, who helped to significantly improve the manuscript. We are grateful also to Edward Blunt who improved considerably our English.

Funding Open access funding provided by University of Basel.

Data availability The authors declare that the data supporting the findings of this study are available within the paper. In case raw data files are needed in another format, they are available from the corresponding author upon reasonable request.

References

Alexandrov P, Giuliani G, Zimmermann J-L (2001) Mineralogy, age and fluid geochemistry of the Rila emerald deposit, Bulgaria. Econ Geol 96:1469–1476

Antić MD, Kounov A, Trivić B, Wetzel A, Peytcheva I, von Quadt A (2016) Alpine thermal events in the central Serbo-Macedonian Massif (southeastern Serbia). Int J Earth Sci 105:1485–1505

Balkanska E, Georgiev S, Kounov A, Antić M, Tagami T, Sueoka S, Wijbrans J, Peytcheva I (2022) Low-temperature constraints on

the Alpine thermal evolution of the central parts of the Sredna Gora Zone. Bulgaria Geol Carp 73(1):3–23

Bonev N, Burg J-P, Ivanov Z (2006) Mesozoic-Tertiary structural evolution of an extensional gneiss dome—the Kesebir-Kardamos dome, eastern Rhodope (Bulgaria–Greece). Int J Earth Sci 95:318–340

Bonev N, Marchev P, Moritz R, Collings D (2015) Jurassic subduction zone tectonics of the Rhodope Massif in the Thrace region (NE Greece) as revealed by new U-Pb and $^{40}Ar/^{39}Ar$ geochronology of the Evros ophiolite and high-grade basement rocks. Gondwana Res 27:760–775

Bosse V, Boulvais P, Gautier P, Tiepolo M, Ruffet G, Devidal JL, Cherneva Z, Gerdjikov I, Paquette JL (2009) Fluid-induced disturbance of the monazite Th–Pb chronometer: In situ dating and element mapping in pegmatites from the Rhodope (Greece, Bulgaria). Chem Geol 261:286–302

Bosse V, Cherneva Z, Gautier P, Gerdjikov I (2010) Two partial melting events as recorded by the U-Th-Pb chronometer in monazite: LA-ICPMS in situ dating in metapelites from the Bulgarian Central Rhodopes. XIX Congress of the Carpathian Balkan Geological Association, Thessaloniki, Greece, pp 51–52

Boyanov I, Goranov A (2001) Late Alpine (Palaeogene) superimposed depressions in parts of Southeast Bulgaria. Geol Balc 31:3–6

Braun J (2016) Strong imprint of past orogenic events on the thermochronological record. Tectonophysics 683:325–332

Brun J-P, Sokoutis D (2007) Kinematics of the Southern Rhodope Core Complex (North Greece). Int J Earth Sci 96:1079–1099

Burchfiel BC, Nakov R, Dumurdzanov N, Papanikolaou D, Tzankov T, Serafimovski T, King RW, Kotzev V, Todosov A, Nurce B (2008) Evolution and dynamics of the Cenozoic tectonics of the South Balkan extensional system. Geosphere 4(6):919–938

Burg J-P (2012) Rhodope: from Mesozoic convergence to Cenozoic extension. Review of petro-structural data in the geochronological frame. J Virt Ex 42:1–44

Burg J-P, Ricou L-E, Klain L, Ivanov Z, Dimov D (1995) Crustal-Scale Thrust Complex in the Rhodope Massif. In: Nairn AEM, Ricou L-E, Vrielynck B, Dercourt J (eds) The Tethys Ocean. Springer, Boston, pp 125–149

Burg J-P, Ricou L-E, Ivanov Z, Godfriaux I, Dimov D, Klain L (1996) Syn-metamorphic nappe complex in the Rhodope Massif. Structure and Kinematics Terra Nova 8:6–15

Carrigan CW, Mukasa SB, Haydoutov I, Kolcheva K (2005) Age of Variscan magmatism from the Balkan sector of the orogen, central Bulgaria. Lithos 82:125–147

Carrigan CW, Mukasa SB, Haydoutov I, Kolcheva K (2006) Neoproterozoic magmatism and Carboniferous high-grade metamorphism in the Sredna Gora Zone, Bulgaria: an extension of the Gondwana-derived Avalonian-Cadomian belt? Precambrian Res 147:404–416

Cernjavska S (1977) Palynological studies on Paleogene deposits in south Bulgaria. Geol Balc 7:3–26

Cernjavska S (2000) Palynological analysis of samples from the Padala formation. Geol Balc 30(1–2):18–19

Cherneva Z, Ovtcharova M, Dimov D, von Quadt A (2006) "Baby-granites" in migmatites from Chepinska river valley, Western Rhodope - geochemistry and U-Pb isotope dating on monazite and zircon. Bulgarian Geological Society, National Conference with International Participation "Geosciences 2006", Sofia, Bulgaria, pp 205–208

Cohen KM, Finney SC, Gibbard PL, Fan J-X (2022) The ICS International Chronostratigraphic Chart. Episodes 36:199–204

Collings D, Savov I, Maneiro K, Baxter E, Harvey J, Dimitrov I (2016) Late Cretaceous UHP metamorphism recorded in kyanite–garnet schists from the Central Rhodope Mountains, Bulgaria. Lithos 246–247:165–181

Dabovski H, Synnyovsky D, Vasilev E, Dimitrova E (2009) Upper Cretaceous geology—Stratigraphy. In: Zagorchev I, Dabovski C, Nikolov T (eds) Geology of Bulgaria, vol II. Mesozoic geology. "Prof. Marin Drinov" Academic Publishing House, Sofia, pp 15–37

Danišík M, Gorinova T, Georgiev N, Kuhlemann J (2014) Cenozoic exhumation of the Rila Mts. (Bulgaria) as constrained by multisystem low-temperature thermochronology. XX Congress of the Carpathian Balkan Geological Association, Tirana, Albania, pp 24–26

Dimitrova E (1960) Petrology of crystalline basement of Northwestern Rila Mountain. Trav Geol Bulg Ser Geochem Met Nonmet 1:199–257

Dimov D, Damianova K (1996) Synmetamorphic tectonic units in Norhwest Rila. Rev Bulg Geol Soc 57(2):25–30

Dimov D, Georgiev N (2000) Exhumation related milonitization of granitoides—an example from the Rila-Rhodope Batholith. Ann Univ Sofia Geol 1(92):23–27

Dinter DA (1998) Late Cenozoic extension of the Alpine collisional orogen, northeastern Greece: origin of the north Aegean basin. Geol Soc Am Bull 110(9):1208–1230

Dinter DA, Royden L (1993) Late Cenozoic extension in northeastern Greece: Strymon Valley detachment system and Rhodope metamorphic core complex. Geology 21:45–48

Dumurdzanov N, Serafimovski T, Burchfiel BC (2005) Cenozoic tectonics of Macedonia and its relation to the South Balkan extensional regime. Geosphere 1:1–22

Fossen H, Rotevatn A (2016) Fault linkage and relay structures in extensional settings—a review. Earth Sci Rev 154:14–28

Froitzheim N, Jahn-Awe S, Frei D, Wainwright AN, Maas R, Georgiev N, Nagel TJ, Pleuger J (2014) Age and composition of meta-ophiolite from the Rhodope Middle Allochthon (Satovcha, Bulgaria): a test for the maximum-allochthony hypothesis of the Hellenides. Tectonics 33:1477–1500

Gautier P, Bosse V, Cherneva Z, Didier A, Gerdjikov I, Tiepolo M (2017) Polycyclic alpine orogeny in the Rhodope metamorphic complex: the record in migmatites from the Nestos shear zone (N. Greece). Bull Soc Géol Fr 188(36):1–28

Georgiev N, Pleuger J, Froitzheim N, Sarov S, Jahn-Awe S, Nagel TJ (2010) Separate Eocene-Early Oligocene and Miocene stages of extension and core complex formation in the Western Rhodopes, Mesta Basin, and Pirin Mountains (Bulgaria). Tectonophysics 487:59–84

Georgiev N, Froitzheim N, Cherneva Z, Frei D, Grozdev V, Jahn-Awe S, Nagel TJ (2016) Structure and U-Pb zircon geochronology of an Alpine nappe stack telescoped by extensional detachment faulting (Kulidzhik area, Eastern Rhodopes, Bulgaria). Int J Earth Sci 105:1985–2012

Georgieva M, Bosse V, Cherneva Z, Kirilova M (2011) Products of HP melting in Chepelare shear zone, Central Rhodope, Bulgaria—petrology, P-T estimates and U-Th-Pb dating. Bulgarian Geological Society. In: National Conference with International Participation "Geosciences 2011", Sofia, Bulgaria, pp 55–56

Gerdjikov I, Gautier P (2006) Processes of crust's extension along the northern margin of the Rhodopes and Rila. Geol Miner Resour 6:23–26

Gerdjikov I, Gautier P, Cherneva Z, Ruffet G (2006) The northwestern segment of the North Rhodopean extensional system and related fabrics in the Rila Rhodopean batholith. Bulgarian Geological Society. In: National Conference with International Participation "Geosciences 2006", Sofia, Bulgaria, pp 79–82

Gerdjikov I, Ruffet G, Lazarova A, Vangelov D, Balkanska E, Bonev K (2010) $^{40}Ar/^{39}Ar$ geochronologic constrains of a Variscan transpression in Central Stara planina Mountain. Bulgarian Geological Society, National Conference with International Participation "Geosciences 2010", Sofia, Bulgaria, pp 107–108

Gleadow AJW, Duddy IR (1981) A natural long-term track annealing experiment for apatite. Nucl Tracks 5:169–174

Gorinova T (2020) Structural characteristic and tectonometamorphic evolution of the rocks of the high-grade basement of Northwest Rila Mountain, Bulgaria. Ph.D. Thesis, Sofia University, Sofia, Bulgaria

Gorinova T, Georgiev N, Cherneva Z, Naydenov K, Grozdev V (2019) A kinematics and time of emplacement of the upper Allochthon of the Rhodope Metamorphic complex: evidence from the Rila Mountains, Bulgaria. Int J Earth Sci 108:2129–2152

Gunnell Y, Calvet M, Meyer B, Pinna-Jamme R, Bour I, Gautheron C, Carter A, Dimitrov D (2017) Cenozoic landforms and post-orogenic landscape evolution of the Balkanide orogen: evidence for alternatives to the tectonic denudation narrative in southern Bulgaria. Geomorphology 276:203–221

Harrison TM, Duncan I, McDougall I (1985) Diffusion of ^{40}Ar in biotite: temperature, pressure and compositional effects. Geochim Cosmochim Acta 49:2461–2468

Harkovska A, Marchev P, Pecskay Z (1998) Paleogene magmatism in the Central Rhodope area, Bulgaria—a review and new data. Acta Vulcanol 10(2):199–216

Ivanov Ž (2017) Tectonics of Bulgaria. Sofia University Press, Sofia, pp 1–331

Ivanov Z, Dimov D, Sarov S (2000) Structure of the Cenral Rhodopes. In: Structure, Alpine evolution and mineralizations of the Central Rhodopes area (South Bulgaria). Guide to excursion B. ABCD–GEODE 2000 Workshop, Borovets, Bulgaria, University Press "St. Kliment Ohridski", pp 6–21

Jahn-Awe S, Pleuger J, Frei D, Georgiev N, Froitzheim N, Nagel TJ (2012) Time constraints for low-angle shear zones in the Central Rhodopes (Bulgaria) and their significance for the exhumation of high-pressure rocks. Int J Earth Sci 101:1971–2004

Janák M, Froitzheim N, Georgiev N, Nagel TJ, Sarov S (2011) P-T evolution of kyanite eclogite from the Pirin Mountains (SW Bulgaria): implications for the Rhodope UHP metamorphic complex. J Metamorph Geol 29:317–332

Kamenov B, Peytcheva I, Klain L, Kostitsin Y, Salnikova E (1999) Rila-West Rhodopes Batholith: petrological and geochemical constraints for its composite character. Geochem Mineral Petrogr 36:3–27

Kilias A, Falalakis G, Sfeikos A, Papadimitriou E, Vamvaka A, Gkarlaouni C (2013) The Thrace basin in the Rhodope province of NE Greece—a tertiary supradetachment basin and its geodynamic implications. Tectonophysics 595–596:90–105

Kirchenbaur M, Pleuger J, Jahn-Awe S, Nagel TJ, Froitzheim N, Fonseca ROC, Münker C (2012) Timing of high-pressure metamorphic events in the Bulgarian Rhodopes from Lu–Hf garnet geochronology. Contrib Mineral Petrol 163:897–921

Kolcheva K, Cherneva Z (1999) Metamorphic evolution of metapelites from the North-western Rila mountain. Geochem Mineral Petrol 36:45–66

Kounov A, Seward D, Bernoulli D, Burg J-P, Ivanov Z (2004) Thermotectonic evolution of an extensional dome: the Cenozoic Osogovo-Lisets core complex (Kraishte zone, western Bulgaria). Int J Earth Sci 93:1008–1024

Kounov A, Seward D, Burg J-P, Bernoulli D, Ivanov Z, Handler R (2010) Geochronological and structural constraints on the Cretaceous thermotectonic evolution of the Kraishte zone, western Bulgaria. Tectonics 29:2002

Kounov A, Wüthrich E, Seward D, Burg J-P, Stockli D (2015) Low-temperature constraints on the Cenozoic thermal evolution of the Southern Rhodope Core Complex (Northern Greece). Int J Earth Sci 104:1337–1352

Kounov A, Gerdjikov I, Vangelov D, Balkanska E, Lazarova A, Georgiev S, Blunt E, Stockli D (2018) First thermochronological constraints on the Cenozoic extension along the Balkan fold-thrust belt (Central Stara Planina Mountains, Bulgaria). Int J Earth Sci 107:1515–1538

Kounov A, Seward D, Burg J-P, Stockli D, Wüthrich E (2020) Cenozoic thermal evolution of the Central Rhodope Metamorphic Complex (Southern Bulgaria). Int J Earth Sci 109:1589–1611

Krohe A, Mposkos E (2002) Multiple generations of extensional detachments in the Rhodope Mountains (northern Greece): evidence of episodic exhumation of high-pressure rocks. In: Blundell DJ, Neubauer F, von Quadt A (eds) The timing and location of major ore deposits in an evolving orogen. Geological Society, London, Special Publication 204, pp 151–178

Kydonakis K, Moulas E, Chatzitheodoridis E, Brun J-P, Kostopoulos D (2015) First-report on Mesozoic eclogite-facies metamorphism preceding Barrovian overprint from the western Rhodope (Chalkidiki, northern Greece). Lithos 220–223:147–163

Lee JY, Marti K, Severinghaus K, Kawamura K, Yoo HS, Lee JB, Kim JS (2006) A redetermination of the isotopic abundances of atmospheric Ar. Geochim Cosmochim Acta 70:4507–4512

Liati A, Gebauer D, Wysoczanski R (2002) U-Pb SHRIMP-dating of zircon domains from UHP garnet-rich mafic rocks and late pegmatoids in the Rhodope zone (N Greece); evidence for Early Cretaceous crystallization and Late Cretaceous metamorphism. Chem Geol 184:281–299

Liati A (2005) Identification of repeated Alpine (ultra) high-pressure metamorphic events by U-Pb SHRIMP geochronology and REE geochemistry of zircon: the Rhodope zone of Northern Greece. Contrib Mineral Petrol 150:608–630

Lister GS, Davis GA (1989) The origin of metamorphic core complexes and detachment faults formed during Tertiary continental extension in the northern Colorado River region, USA. J Struct Geol 11:65–94

Marchev P, Kaiser-Rohrmeier M, Heinrich C, Ovtcharova M, von Quadt A, Raicheva R (2005) 2: Hydrothermal ore deposits related to post-orogenic extensional magmatism and core complex formation: the Rhodope Massif of Bulgaria and Greece. Ore Geol Rev 27:53–89

Marchev P, Raicheva R, Georgiev S, Savov IP, Jelev D (2022) Formation of ultrapotassic magma via crustal contamination and hybridization of mafic magma: an example from the Stomanovo monzonite, Central Rhodope Massif, Bulgaria. Geol Mag 159:81–96

Marinova R, Zagorchev I (1991) Geological map of the Republic of Bulgaria in scale 1:100 000, K-34–71 (Blagoevgrad) map sheet; Explanatory note for the geological map of the Republic of Bulgaria in scale 1:1010 000, K-34–71 (Blagoevgrad) map sheet. Geological Institute of BAS, Enterprise of Geophysical Surveys and Geological Mapping, Sofia pp 1–52

Miladinova I, Froitzheim N, Sandmann S, Nagel TJ, Georgiev N, Münker C (2013) Middle Triassic eclogite in the Rila Mountains (Rhodope Upper Allochthon, Bulgaria): a vestige of Palaeotethys subduction? In: 11th Workshop on Alpine Geological Studies and 7th IFAA, Berichte Geologie, Schladming, Austria, pp 65

Nagel TJ, Schmidt S, Janák M, Froitzheim N, Jahn-Awe S, Georgiev N (2011) The exposed base of a collapsing wedge: The Nestos Shear Zone (Rhodope Metamorphic Province, Greece). Tectonics 30:TC4009

Naydenov K, Sarov S, Voynova E, Jelezarski T, Georgieva I, Nikolov D, Petrov N, Markov N, Marinova R (2008) Geological map of the Republic of Bulgaria in scale 1:50 000, K-34–72-B (Kostenets) map sheet; Explanatory note for the geological map of the Republic of Bulgaria in scale 1:50 000, K-34–72-B (Kostenets) map sheet. Ministry of environment and waters, Bulgarian National Geological Survey, Sofia, pp 1–42

Naydenov K, von Quadt A, Peytcheva I, Sarov S, Dimov D (2009) U-Pb zircon dating of metamorphic rocks in the region of

Kostenets-Kozarsko villages: constraints on the tectonic evolution of the Maritsa strike-slip shear zone. Rev Bulg Geol Soc 70(1–3):5–21

Passchier CW, Trouw AJ (2005) Microtectonics. Springer, Berlin

Petrík I, Janák M, Froitzheim N, Georgiev N, Yoshida K, Sasinková V, Konečný P, Milovská S (2016) Triassic to Early Jurassic (c. 200 Ma) UHP metamorphism in the Central Rhodopes: evidence from U-Pb-Th dating of monazite in diamond-bearing gneiss from Chepelare (Bulgaria). J Metamorph Geol 34:265–291

Peytcheva I, Von Quadt A, Naydenov K, Sarov S, Dimov D, Voinova E. (2007) U-Pb zircon-xenotime-monazite dating and Hf-isotope tracing to distinguish Cretaceous and Paleogene granitoids in the Western Rhodopes and Rila Mountain. Bulgarian Geological Society, National Conference with International Participation "Geosciences 2007", Sofia, Bulgaria, pp 89–91

Peytcheva I, von Quadt A, Sarov S, Voinova E, Kolcheva K (2009) Ordovician protoliths of metamorphic rocks in Eastern Pirin—Western Rhodopes: Are they part of the Ograzhden Unit? Bulgarian Geological Society. In: National Conference with International Participation "Geosciences 2009", Sofia, Bulgaria, pp 17–18

Pleuger J, Georgiev N, Jahn-Awe S, Froitzheim N, Valkanov N (2011) Kinematics of Palaeogene low-angle extensional faults and basin formation along the eastern border of the Central Rhodopes (Bulgaria). Zeitschrift Der Dtsch Gesellschaft Fur Geowissenschaften 162:171–192

Popov M, Ivanov I (2012) Two contrasting U-Pb zircon age determinations of metamorphic rocks in the western part of the Rhodope metamorphic complex. Bulgarian Geological Society. In: National Conference with International Participation "Geosciences 2012", Sofia, Bulgaria, pp 63–64

Popov K, Velichkov D, Popov P (2015) The post-collisional Upper Thracian rift system (Bulgaria) and the formed exogenous uranium deposits. Part 1—Lithostratigraphy and tectonic. Rev Bulg Geo Soc 76(2–3):35–49

Ricou L-E, Burg J-P, Godfriaux I, Ivanov Z (1998) Rhodope and Vardar: the metamorphic and the olistostromic paired belts related to the Cretaceous subduction under Europe. Geodin Acta 1(6):285–309

Rahn MK, Seward D (2000) How many track lengths do we need? OnTrack 10(20):12–15

Harrison TM, Célérier J, Aikman AB, Hermann J, Heizler MT (2009) Diffusion of ^{40}Ar in muscovite. Geochim Cosmochim Acta 73:1039–1051

Sarov S, Petrov N, Voinova E, Nedkova K, Naydenov K, Georgieva I, Nikolov D, Kolcheva K (2006) Data on strike-slip shearings in the low-grade methamorphic sections (Trachian Unit) in the northern part of the Central Rhodopes. Bulgarian Geological Society. In: National Conference with International Participation "Geosciences 2006", Sofia, Bulgaria, pp 102–105

Sarov S, Voinova E, Moskovski S, Jelezarski T, Georgieva I, Nikolov D, Naydenov K, Petrov N, Markov N, Marinova R (2008a) Geological map of the Republic of Bulgaria in scale 1:50 000, K-35–61-V (Kostandovo) map sheet; Explanatory note for the geological map of the Republic of Bulgaria in scale 1:50 000, K-35–61-V (Kostandovo) map sheet. Ministry of environment and waters, Bulgarian National Geological Survey, Sofia, pp 1–43

Sarov S, Naydenov K, Voinova E, Moskovski S, Jelezarski T, Georgieva I, Nikolov D, Petrov N, Markov N, Marinova R (2008b) Geological map of the Republic of Bulgaria in scale 1:50 000, K-35–61-G (Peshtera) map sheet; Explanatory note for the geological map of the Republic of Bulgaria in scale 1:50 000, K-35–61-G (Peshtera) map sheet. Ministry of environment and waters, Bulgarian National Geological Survey, Sofia, pp 1–54

Sarov S, Moskovski S, Jelezarski T, Georgiev N, Voynova E, Nikolov D, Georgieva I, Valev V, Markov N (2010) Geological map of the Republic of Bulgaria in scale 1:50 000, K-34–84-G (Kovachevitsa) map sheet; Explanatory note for the geological map of the Republic of Bulgaria in scale 1:50 000, K-34–84-G (Kovachevitsa) map sheet. Ministry of environment and waters, Bulgarian National Geological Survey, Sofia, pp 1–43

Sarov S, Moskovski S, Jelezarski T, Voynova E, Nikolov D, Georgieva I, Valev V, Markov N (2011a) Geological map of the Republic of Bulgaria in scale 1:50 000, K-34–71-B (Sapareva Banya) map sheet; Explanatory note for the geological map of the Republic of Bulgaria in scale 1:50 000, K-34–71-B (Sapareva Banya) map sheet. Ministry of environment and waters, Bulgarian National Geological Survey, Sofia, pp 1–48

Sarov S, Moskovski S, Jelezarski T, Voynova E, Nikolov D, Georgieva I, Valev V, Markov N (2011b) Geological map of the Republic of Bulgaria in scale 1:50 000, K-34–71-A (Dupnitsa) map sheet; Explanatory note for the geological map of the Republic of Bulgaria in scale 1:50 000, K-34–71-A (Dupnitsa) map sheet. Ministry of environment and waters, Bulgarian National Geological Survey, Sofia, pp 1–48

Schaen AJ, Jicha BR, Hodges KV, Vermeesch P, Stelten ME, Mercer CM, Phillips D, Rivera TA, Jourdan F, Matchan EL, Hemming SR, Morgan LE, Kelley SP, Cassata WS, Heizler MT, Vasconcelos PM, Benowitz JA, Koppers AAP, Mark DF, Niespolo EM, Sprain CJ, Hames WE, Kuiper KF, Turrin BD, Renne PR, Ross J, Nomade S, Guillou H, Webb LE, Cohen BA, Calvert AT, Joyce N, Ganerød M, Wijbrans J, Ishizuka O, He H, Ramirez A, Pfänder JA, Lopez-Martínez M, Qiu H, Singer BS (2021) Interpreting and reporting ^{40}Ar/^{39}Ar geochronologic data. Geol Soc Am Bull 3–4:461–487

Schmid SM, Fügenschuh B, Kounov A, Maţenco L, Nievergelt P, Oberhänsli R, Pleuger J, Schefer S, Schuster R, Tomljenović B, Ustaszewski K, van Hinsbergen DJJ (2020) Tectonic units of the Alpine collision zone between Eastern Alps and western Turkey. Gondwana Res 78:308–374

Shipkova KA (1999) Synmetamorphic deformations in the NW Rila mountain. Ph.D. Thesis, Sofia University, Sofia, Bulgaria, pp 225

Shipkova K, Ivanov Z (2000) The Djerman Detachment Fault—an effect of the Late Tertiary extension in the north-west part of the Rhodope Massif. C R Acad Bulg Sci 53(2):81–84

Stipp M, Stünitz H, Heilbronner R, Schmid SM (2002) The eastern Tonale fault zone: a "natural laboratory" for crystal plastic deformation of quartz over a temperature range from 250 to 700 C. J Struct Geol 24(12):1861–1884

Stübner K, Drost K, Schoenberg R, Böhme M, Starke J, Ehlers TA (2016) Asynchronous timing of extension and basin formation in the South Rhodope core complex, SW Bulgaria, and northern Greece. Tectonics 35:136–159

Tueckmantel C, Schmidt S, Neisen M, Georgiev N, Nagel TJ, Froitzheim N (2008) The Rila-Pastra Normal Fault and multi-stage extensional unroofing in the Rila Mountains (SW Bulgaria). Swiss J Geosci 101:295–310

Turpaud P, Reischmann T (2010) Characterisation of igneous terranes by zircon dating: implications for UHP occurrences and suture identification in the Central Rhodope, northern Greece. Int J Earth Sci 99:567–591

Valkov V, Antova N, Doncheva K (1989) The granitoids in Rita-West Rhodope batholith. Geol Balc 19(2):21–54

Valkova NP, Spiridonov HB (1979) The Marica deep fault during the Neozoic in the area between Varvara village, Pazardžik district and the town of Kostenec. Rev Bulg Geol Soc 40(2):167–173

von Quadt A, Peytcheva I (2005) The southern extension of the Srednogorie type Upper Cretaceous in Rila-Western Rhodopes: constraints from isotpe-geochronological geochemical data. Bulgarian Geological Society. In: National Conference with

International Participation “Geosciences 2005”, Sofia, Bulgaria, pp 113–116

Wolff R, Hetzel R, Dunkl I, Anczkiewicz AA, Pomella H (2020) Fast cooling of normal-fault footwalls: rapid fault slip or thermal relaxation? Geology 48:333–337

Zagorchev I (1992) Neotectonic development of the Struma (Kraistid) Lineament, southwest Bulgaria and northern Greece. Geol Mag 129:197–222

Zagorchev I (1996) Pre-Palaeogene Alpine tectonic units and terranes in the border area of SW Bulgaria and Yugoslavia. In: Knezevic V, Krstic B (eds) Terranes of Serbia. Belgrade, pp 81–86

Zagorchev I, Popov P, Ruseva M (1989) Paleogene stratigraphy in a part of SW Bulgaria. Geol Balc 19:41–69 (In Russian, English abstract)

Zagorchev I, Balica C, Kozhoukharova E, Balintoni I, Sabau G, Negulescu E (2014) Palaeogene igneous evolution of the Rhodopes. Bulgarian Geological Society, National Conference with International Participation “Geosciences 2014”, Sofia, Bulgaria, pp 35–36